J. Fluid Mech. (2012), *vol.* 712, *pp.* 129–168.
doi:10.1017/jfm.2012.404

Enskog kinetic theory for monodisperse gas–solid flows

V. Garzó[1], S. Tenneti[2], S. Subramaniam[2] and C. M. Hrenya[3]†

[1] Departamento de Física, Universidad de Extremadura, E-06071 Badajoz, Spain

[2] Department of Mechanical Engineering, Iowa State University, Ames, IA 50011, USA

[3] Department of Chemical and Biological Engineering, University of Colorado, Boulder, CO 80309, USA

(Received 21 June 2011; revised 28 June 2012; accepted 7 August 2012;
first published online 27 September 2012)

The Enskog kinetic theory is used as a starting point to model a suspension of solid particles in a viscous gas. Unlike previous efforts for similar suspensions, the gas-phase contribution to the instantaneous particle acceleration appearing in the Enskog equation is modelled using a Langevin equation, which can be applied to a wide parameter space (e.g. high Reynolds number). Attention here is limited to low Reynolds number flow, however, in order to assess the influence of the gas phase on the constitutive relations, which was assumed to be negligible in a previous analytical treatment. The Chapman–Enskog method is used to derive the constitutive relations needed for the conservation of mass, momentum and granular energy. The results indicate that the Langevin model for instantaneous gas–solid force matches the form of the previous analytical treatment, indicating the promise of this method for regions of the parameter space outside of those attainable by analytical methods (e.g. higher Reynolds number). The results also indicate that the effect of the gas phase on the constitutive relations for the solid-phase shear viscosity and Dufour coefficient is non-negligible, particularly in relatively dilute systems. Moreover, unlike their granular (no gas phase) counterparts, the shear viscosity in gas–solid systems is found to be zero in the dilute limit and the Dufour coefficient is found to be non-zero in the elastic limit.

Key words: granular media, particle/fluid flow, suspensions

1. Introduction

The kinetic-theory-based description of rapid granular flows (i.e. those in which the role of the interstitial fluid is neglected) has been an active area of research for the past several decades (Campbell 1990; Goldhirsch 2003; Brilliantov & Pöschel 2004). Sinclair & Jackson (1989) first extended this analogy to rapid gas–solid flows in vertical tubes to explain the ubiquitous ‘core–annulus’ flow, in which the solids are observed to have a higher concentration near the pipe wall (annulus), while the centre of the pipe (core) remains relatively dilute. This extension of the kinetic-theory analogy to gas–solid systems is appropriate for relatively massive particles (i.e. high Stokes number) engaging in nearly instantaneous collisions. Such systems occur in a wide range of engineering operations, including the riser section

† Email address for correspondence: hrenya@colorado.edu

of a circulating fluidized bed, pneumatic conveying systems, and bubbling fluidized beds. Correspondingly, the further development and application of kinetic-theory-based models to high-velocity gas–solid systems has mushroomed over the last twenty years (Gidaspow 1994; Jackson 2000; Koch & Hill 2001; Gidaspow & Jiradilok 2009; Pannala, Syamlal & O'Brien 2011). Important research thrusts have included, but are not limited to, the effects of gas-phase turbulence, clustering instabilities, polydispersity, cohesion, non-spherical particles, and friction.

The aim of the current effort is on the fluid–solid interaction force, $\boldsymbol{F}_{fluid}$, present in high-velocity gas–solid flows. Particular emphasis is placed on the incorporation of $\boldsymbol{F}_{fluid}$ into the continuum description of the solid phase (which can later be coupled with gas-phase mass and momentum balances for a complete description of the gas–solid system). Before describing related previous works, it is worthwhile to introduce the physical picture associated with this interaction force. Mathematically, this fluid–solid force is the sum of normal ($\boldsymbol{F}_n$) and tangential ($\boldsymbol{F}_t$) forces experienced by the particle at its surface. For the case of fluid flow in the z-direction around a stationary sphere, the z-component of this interaction force is given by

$$\begin{aligned} F_{fluid,z} &= F_{n,z} + F_{t,z} \\ &= \int_0^{2\pi}\int_0^{\pi} (-p|_{r=R}\cos\theta)\, R^2 \sin\theta \,\mathrm{d}\theta \,\mathrm{d}\varphi \\ &\quad + \int_0^{2\pi}\int_0^{\pi} (\tau_{r\theta}|_{r=R}\sin\theta)\, R^2 \sin\theta \,\mathrm{d}\theta \,\mathrm{d}\varphi, \end{aligned} \tag{1.1}$$

where p is the fluid pressure, $\boldsymbol{\tau}$ is the (Newtonian) fluid stress, and R is the particle radius. Accordingly, $\boldsymbol{F}_{fluid}$ depends on both the pressure and velocity-gradient fields at the particle surface. As an illustration of the former, the pressure field is given in figure 1(*b*), which shows a single motionless particle suspended in mean (far-away) fluid flow (or, equivalently, a sphere moving in the same direction as mean fluid flow). For this simple case, the fluid–solid force on the particle is typically expressed as $\boldsymbol{F}_{fluid} = \beta(\boldsymbol{U}_g - \boldsymbol{U})$, where β is a drag coefficient that depends on the particle Reynolds number, $\boldsymbol{U}_g$ is the mean gas velocity and $\boldsymbol{U}$ is the (mean) particle velocity. A slightly more complex situation is depicted in figure 1(*c*), where the particle is now moving in a different direction than the mean fluid flow, as indicated by the arrow, but still unaffected by neighbour particle effects. The presence of such particle motion leads to a change in the pressure field (and velocity-gradient field, not shown) at the particle surface, thereby causing a change in $\boldsymbol{F}_{fluid}$ (equation (1.1)). An even more complex scenario is shown in figure 1(*d*), where the presence of surrounding moving particles causes a continual change in the pressure (and velocity) field around the particle of interest, resulting in a dynamic gas–solid interaction force. Accordingly, the fluid–solid force experienced by a single particle can be decomposed into the contributions arising from mean slip velocity between the solid and gas phases (figure 1*b*), instantaneous particle velocity fluctuations with respect to mean velocity of the solid phase (figure 1*c*), and the contribution due to neighbour particle effects (figure 1*d*). It is worthwhile to note that this last system (figure 1*d*) best captures the interactions occurring in the practical gas–solid systems mentioned above (e.g. fluidized beds).

Early efforts to incorporate the effects of $\boldsymbol{F}_{fluid}$ into the continuum description of gas–solids flows took a relatively straightforward approach, while more recent studies have continued to increase the level of rigour. In particular, the first gas–solid models

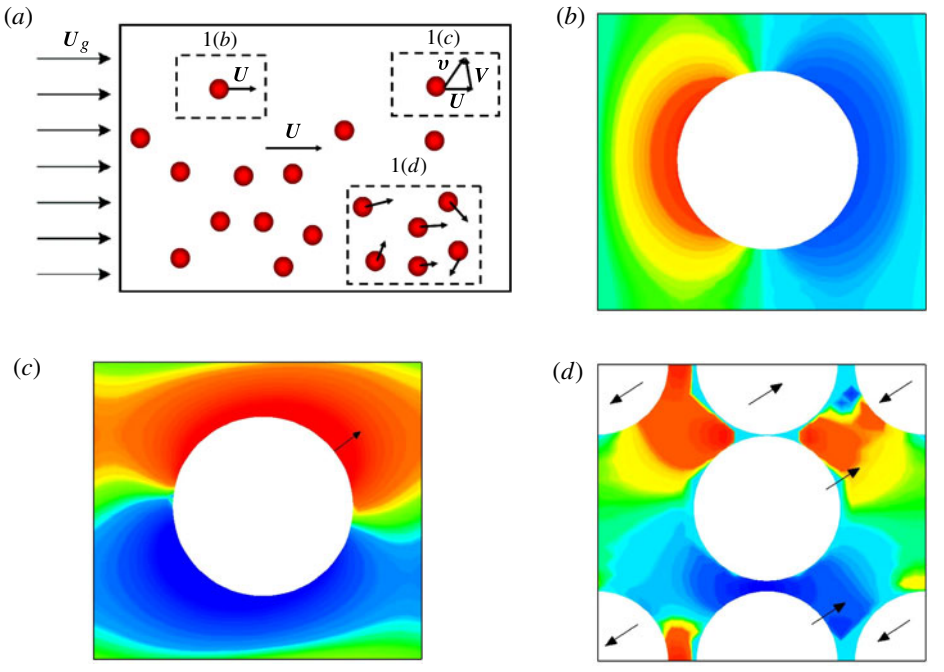

FIGURE 1. (Colour online) (*a*) Illustration of different contributions to the instantaneous gas–solid force in a suspension with mean fluid velocity $\boldsymbol{U}_g$ and mean particle velocity $\boldsymbol{U}$. Pressure contours are shown for (*b*) a single particle far away from its neighbours and moving with a velocity equal to the mean particle velocity, (*c*) a particle moving in a different direction than the mean fluid flow and far from its neighbours, and (*d*) a collection of particles moving in different directions. The pressure contours are obtained from particle-resolved direct numerical simulations (PR–DNS) for a gas–solid suspension that corresponds to a solid volume fraction of 0.2 and mean-flow Reynolds number 0.01.

described the solid phase according to the mass, momentum, and granular energy balances developed for granular (no fluid) systems, with the only modification being the addition of a (mean) drag force onto the momentum balance. This drag force was typically described using empirical relations obtained via settling experiments (Richardson & Zaki 1954; Wen & Yu 1966; Gidaspow 1994), in which the force is a function of the relative mean velocity between the two phases and the solid volume fraction ϕ (i.e. $\boldsymbol{F}_{fluid} = \beta(\boldsymbol{U}_g - \boldsymbol{U})$, where β is a function of $\boldsymbol{U}_g - \boldsymbol{U}$ and ϕ). It is worthwhile to note that with this approach, the granular energy balance does not contain any new terms arising from fluid-phase effects, nor do any of the constitutive relations for the solid phase (stress, heat flux, or collisional cooling rate) incorporate fluid-phase effects. As an example, see the pioneering gas–solid model proposed by Sinclair & Jackson (1989), who used the governing balances of Anderson & Jackson (1967) and the granular theory of Lun & Savage (2003). A more exact approach has since been adopted, in which fluid-phase effects are incorporated at the starting point of the derivation for the solid-phase balances and their constitutive equations, namely the kinetic equation (e.g. Boltzmann or Enskog kinetic equation)

$$\partial_t f + \boldsymbol{v} \cdot \boldsymbol{\nabla} f + \frac{\partial}{\partial \boldsymbol{v}} \cdot \left[\left(\frac{\boldsymbol{F}_{fluid}}{m} \right) f \right] + \boldsymbol{g} \cdot \frac{\partial f}{\partial \boldsymbol{v}} = J[f, f], \tag{1.2}$$

where f is the one-particle velocity distribution function, $\boldsymbol{v}$ is the instantaneous particle velocity, m is the particle mass, $\boldsymbol{g}$ is the gravity vector, and $J[f,f]$ is the collisional operator. It is important to note here that $\boldsymbol{F}_{fluid}(\boldsymbol{r},\boldsymbol{v},t)$ is a function of the instantaneous particle velocity and can vary in both time and space. Strictly speaking, then, $\boldsymbol{F}_{fluid}$ is an instantaneous force rather than a mean force, where a mean force is one that depends on the hydrodynamic, or mean, fields. Although not strictly correct, the treatment of $\boldsymbol{F}_{fluid}$ as a mean force is considerably easier since it can be taken outside the differential in (1.2). Along these lines, and following from the earlier discussion surrounding figure 1, different approximations for $\boldsymbol{F}_{fluid}$ have been made, leading to differences in the balance equations appearing in the literature.

Consider first the simplest case, where $\boldsymbol{F}_{fluid}$ is approximated as a mean force, namely $\boldsymbol{F}_{fluid} = \beta(\boldsymbol{U}_g - \boldsymbol{U})$, where β is a function of hydrodynamic (mean) variables (figure 1*a*). For this treatment, a mean drag force will appear in the solid-phase momentum balance, consistent with the treatment described in the previous paragraph (Sinclair & Jackson 1989), but no terms appear in the granular energy equation. Next, consider an approximation which accounts for the fluctuation in particle velocity (figure 1*b*) via $\boldsymbol{F}_{fluid} = \beta(\boldsymbol{U}_g - \boldsymbol{v})$, and is thus a function of the instantaneous particle velocity $\boldsymbol{v}$, though β remains a function of the hydrodynamic (mean) fields only. In this case, an additional sink term (which is proportional to β) arises in the granular energy balance due to viscous drag (see e.g. Koch 1990). In a third and improved approximation, fluctuations in both phases are considered in the fluid-force relation (figure 1*c*), namely $\boldsymbol{F}_{fluid} = \beta(\boldsymbol{v}_g - \boldsymbol{v})$, where $\boldsymbol{v}_g$ is the instantaneous gas velocity and with β again typically treated as a function of mean variables. This treatment leads to an additional source term in the granular energy balance arising from fluid-dynamic interactions (see e.g. Gidaspow 1994). However, this approximation leads to a single-point fluid-particle velocity covariance that Xu & Subramaniam (2006) have shown to be inconsistent for finite particle size.

In addition to the aforementioned impact of the $\boldsymbol{F}_{fluid}$ treatment on the balance equations, the form of $\boldsymbol{F}_{fluid}$ will also impact the constitutive relations for the solid-phase quantities (shear stress, heat flux, and collisional cooling rate), as these are also derived from the kinetic equation (1.2). The incorporation of such effects into the constitutive relations has received less attention in the literature. Several groups (Ma & Ahmadi 1988; Balzer, Boelle & Simonin 1995; Lun & Savage 2003) have derived the constitutive relations using a description of $\boldsymbol{F}_{fluid}$ which depends on the instantaneous fluid ($\boldsymbol{v}_g$) and solid ($\boldsymbol{v}$) velocities. With regard to $\boldsymbol{v}_g$, it is worth noting that these works have included velocity fluctuations arising from fluid-phase turbulence. Other groups (Février, Simonin & Squires 2005; Simonin *et al.* 2006; Zaichik, Simonin & Alipchenkov 2009) have also incorporated the effect of turbulent gas-phase velocity fluctuations on the one-particle velocity distribution function in the regime of dilute, sub-Kolmogorov size particles. The type of fluctuations depicted in figure 1(*c*), on the other hand, do not require the presence of turbulent instabilities. More specifically, for the system of figure 1(*c*), the presence of numerous particles moving in different directions will lead to continually changing fluid-dynamic interactions between particles (i.e. fluctuations in the fluid velocity and pressure fields) even at low Reynolds number. Finally, and perhaps more importantly, a common assumption in works that incorporate gas- and/or solid-phase fluctuations is that the basic form of the mean fluid force ($\boldsymbol{F}_{fluid} = \beta(\boldsymbol{U}_g - \boldsymbol{U})$) also holds for its instantaneous counterpart by simply replacing the mean hydrodynamic fields with instantaneous ones (e.g. $\boldsymbol{F}_{fluid} = \beta(\boldsymbol{v}_g - \boldsymbol{v})$). Recent findings by Tenneti *et al.* (2010*b*), however, indicate that such treatments are not appropriate. Figure 2 shows a plot of the streamwise

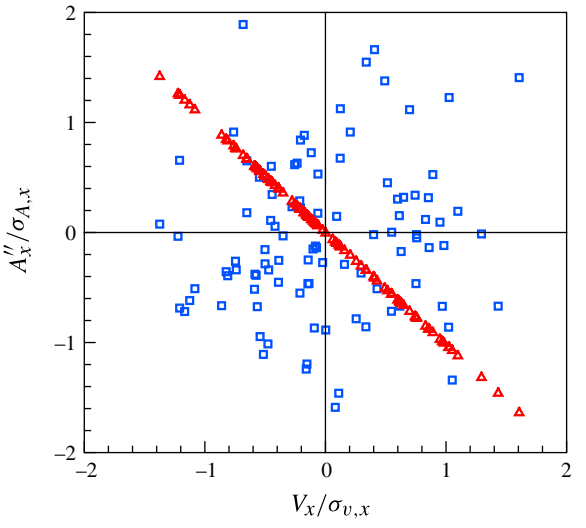

FIGURE 2. (Colour online) Scatter plot of streamwise component of particle acceleration fluctuations $\boldsymbol{A}''$ (normalized by the standard deviation in the particle acceleration distribution σ_A) versus the streamwise component of particle velocity fluctuations $\boldsymbol{V}$ (normalized by the standard deviation in the particle acceleration distribution σ_v). Squares (□) denote the fluctuations in the particle acceleration obtained from PR–DNS of a freely evolving gas–solid suspension corresponding to a solid volume fraction of 0.2, mean-flow Reynolds number of 1.0 and solid-to-fluid density ratio of 1000; upper triangles (△) denote the fluctuations in the particle acceleration predicted by using a model for the fluid-particle force of the form $\boldsymbol{F}_{fluid} = \beta(\boldsymbol{U}_g - \boldsymbol{v})$.

component of fluctuations in particle acceleration $\boldsymbol{A}''$ versus the streamwise component of fluctuations in particle velocity $\boldsymbol{V}$. The fluctuations in the particle acceleration and velocity are defined with respect to their corresponding mean values. The particle acceleration fluctuations are normalized by the standard deviation in the particle acceleration distribution σ_A, while the fluctuations in particle velocity are normalized by the standard deviation in particle velocity distribution σ_V. Square symbols are the particle acceleration fluctuations obtained from particle-resolved direct numerical simulation (PR–DNS) of a freely evolving gas–solid suspension. Triangles are the fluctuations in the particle acceleration predicted by using a model for the fluid-particle force of the form $\boldsymbol{F}_{fluid} = \beta(\boldsymbol{U}_g - \boldsymbol{v})$. It is clear that the joint statistics of the particle acceleration and particle velocity that are crucial for the accurate prediction of the evolution of granular temperature are not well captured by this simplified class of instantaneous models for $\boldsymbol{F}_{fluid}$. Although the model $\boldsymbol{F}_{fluid} = \beta(\boldsymbol{U}_g - \boldsymbol{v})$ results in a sink of granular temperature, it does not account for the source in granular temperature that is responsible for points in quadrants I and III of the fluctuating particle acceleration–velocity scatter plot (see Tenneti, Fox & Subramaniam 2010*a* for details). Moreover, the scatter observed in the particle acceleration fluctuations suggests a stochastic contribution to the fluid-particle force that arises due to the effect of the neighbour particles. For the limiting case of Stokes flow, Koch and co-workers (Koch 1990; Koch & Sangani 1999) were able to correctly describe the acceleration–velocity correlation via analytical means (Koch 1990) and through the use of multipole expansions (Koch & Sangani 1999). Extensions of analytical approaches

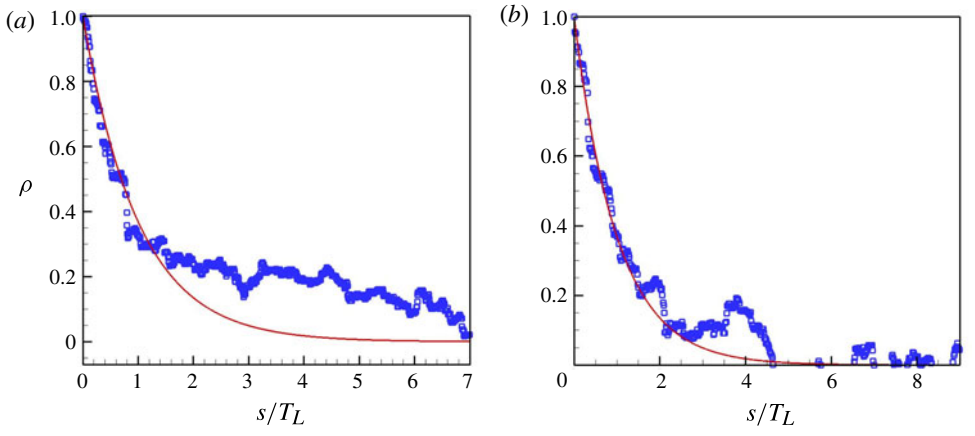

FIGURE 3. (Colour online) Decay of the particle velocity autocorrelation function. (*a*) The particle velocity autocorrelation function computed via PR–DNS (symbols) of freely evolving suspension (volume fraction of 0.2, mean-flow Reynolds number 1.0 and solid-to-fluid density ratio of 1000) compared with the exponential decay predicted by the Langevin model (solid line). (*b*) The same as (*a*) for a suspension with a solid volume fraction of 0.35.

beyond the Stokes limit are difficult since the governing Navier–Stokes equations become nonlinear (Koch & Hill 2001). A further assumption of their analysis was that the influence of gas-phase effects on constitutive relations for the solid phase are negligible at sufficiently large Stokes number; such effects appeared in the balance equations only.

A long-term objective of this effort, then, is to develop a framework in which (i) an accurate instantaneous model for $\boldsymbol{F}_{fluid}$ is developed over a wide range of conditions; and (ii) the resulting $\boldsymbol{F}_{fluid}$ model is used to derive solid-phase balance equations and constitutive relations which fully incorporate gas-phase effects. With regard to (i), the instantaneous gas–solid force is modelled using a Langevin equation because the particle velocity autocorrelation decays exponentially for a range of mean-flow Reynolds numbers (see figure 3). With regard to (ii), the Langevin model for $\boldsymbol{F}_{fluid}$ is then used in the kinetic equation (1.2) to derive the balance equations and constitutive relations. As a first step in this direction, this two-part process is carried out here for low Reynolds numbers. It is important to note that the methodology itself is not restricted to this limit; instead, the focus here is to demonstrate proof-of-concept by (i) comparing the Langevin model for $\boldsymbol{F}_{fluid}$ with previous results for the Stokes limit (Koch 1990; Koch & Sangani 1999), and (ii) using this model to assess the influence of gas-phase effects on the constitutive relations, which were neglected in the analytical treatment. For future extensions to higher Reynolds numbers, the coefficients in the Langevin model can be obtained via PR–DNS, as described by Tenneti *et al.* (2010*a*).

2. Fluid–solid force ($\mathbf{F}_{fluid}$) model

As mentioned above, to develop a closed kinetic equation for the one-particle velocity distribution function $f(\boldsymbol{v})$ (equation (1.2)), a description of the instantaneous particle force $\boldsymbol{F}_{fluid}$ is needed. As the name implies, this instantaneous force is a function of the instantaneous velocities of both the gas and solid phases ($\boldsymbol{v}_g$ and $\boldsymbol{v}$,

respectively), rather than solely the corresponding mean velocities ($\boldsymbol{U}_g$ and $\boldsymbol{U}$). However, consideration of $\boldsymbol{v}_g$ and $\boldsymbol{v}$ for finite particle size would require consideration of two-point statistics (Sundaram & Collins 1999; Xu & Subramaniam 2006). Note that fluctuations in particle velocity may arise from particle interactions (collisional) and/or gas–solid interactions. Although in the special case of Stokes flow the fluid-dynamic interaction arising from neighbour particles can be treated analytically (Koch 1990) for the general case of finite fluid inertia, this is not feasible here.

Therefore, a generalized Langevin model is proposed for the instantaneous impulse as follows:

$$m\,\mathrm{d}\boldsymbol{v} = \boldsymbol{F}_{fluid}\,\mathrm{d}t = -\beta\left(\boldsymbol{U} - \boldsymbol{U}_g\right)\,\mathrm{d}t - \boldsymbol{\gamma}\cdot\boldsymbol{V}\,\mathrm{d}t + m\boldsymbol{B}\cdot\mathrm{d}\boldsymbol{W}, \tag{2.1}$$

where $\boldsymbol{V} = \boldsymbol{v} - \boldsymbol{U}$ is the particle fluctuation (or peculiar) velocity, the vector $\mathrm{d}\boldsymbol{W}$ is a Wiener process increment (stochastic term), and the scalar β and the tensors $\boldsymbol{\gamma}$ and $\boldsymbol{B}$ are the model coefficients. The first term on the right-hand side represents the portion of the drag force arising from the mean motion of particle and solid phase; the second term is traced to fluctuations in particle velocity; the third term is a stochastic model for the change in particle momentum due to shear stress and pressure contributions at the particle surface that arise from the fluid velocity and pressure disturbances caused by neighbour particles. This is one way to extend the analysis of Koch (1990) for point particles in the Stokes flow regime to gas–solid flows with finite fluid inertia and finite particle size. Regarding this third term, note that the instantaneous velocity for the gas phase can be determined rigorously by considering the distribution function for the fluid velocity (in addition to that of the particle velocity, (1.2)). However, such an approach would involve two-point distributions (Sundaram & Collins 1999) which is beyond the current scope, and thus a stochastic model is adopted here. In the following section we outline the assumptions made in this work and justify their validity for the range of physical parameters considered here.

3. Assumptions and their range of validity

3.1. *Range of dimensionless variables*

The assumptions used in this work are relevant to the range of dimensionless physical parameters encountered in a circulating fluidized bed (CFB). The relevant independent set of dimensionless parameters comprises the solid volume fraction ϕ, the mean-flow Reynolds number Re_m, the Reynolds number associated with the particle velocity fluctuations Re_T, and the ratio of the densities of the solid and the gas ρ_s/ρ_g. The mean-flow Reynolds number is defined by

$$Re_m = \frac{(1-\phi)\rho_g\sigma|\Delta\boldsymbol{U}|}{\mu_g}, \tag{3.1}$$

where $\Delta\boldsymbol{U} = \boldsymbol{U} - \boldsymbol{U}_g$, σ is the particle diameter and ρ_g, μ_g are the mass density and dynamic viscosity of the gas, respectively. The Reynolds number associated with the particle velocity fluctuations is defined by

$$Re_T = \frac{\rho_g\sigma}{\mu_g}\sqrt{\frac{T}{m}}, \tag{3.2}$$

where T is the granular temperature (see equation (4.10)) and m is the mass of the particle. It is worth noting that some previous works (Koch 1990) on gas–solid suspensions in the Stokes flow regime cast their results in terms of a Stokes number St

(rather than Re_m and/or Re_T). Here, for a three-dimensional system, we define the two relevant Stokes numbers as

$$St_m = \frac{m|\Delta \boldsymbol{U}|}{6\pi\mu_g R^2}, \tag{3.3}$$

$$St_T = \frac{m\sqrt{T/m}}{6\pi\mu_g R^2}, \tag{3.4}$$

where $R = \sigma/2$ is the radius of a particle. Thus, the relationship between the Stokes numbers and corresponding Reynolds numbers is

$$St_m = \frac{1}{9(1-\phi)}\frac{\rho_s}{\rho_g} Re_m, \tag{3.5}$$

$$St_T = \frac{1}{9}\frac{\rho_s}{\rho_g} Re_T, \tag{3.6}$$

where $\rho_s = 6m/(\pi\sigma^3)$ is the mass density of a particle. Whereas Re_m and Re_T are measures of the fluid inertia (related to mean and fluctuating components of particle motion, respectively) to viscous effects, the Stokes numbers St_m and St_T are measures of particle inertia to fluid viscous effects. The results presented in this paper (see § 8) will give ranges for each of these parameters for the purpose of greater physical understanding (even though they are not independent quantities).

3.2. *Fluid–solid force model*

The most important assumption in this work is that the instantaneous impulse can be modelled using a Langevin equation (see equation (2.1)). The assumption that is implicit in using this model is that the change in particle momentum due to neighbour particle effects occurs on time scales much smaller than those associated with drag due to the mean slip and particle velocity fluctuations. The validity of the Langevin model can be justified by examining the decay of particle velocity autocorrelation function that is computed via PR–DNS (which accounts for all fluid-dynamic interactions exactly). The particle velocity autocorrelation function $\rho(s)$ is defined by

$$\rho(s) = \frac{\langle V_i(t_0) V_i(t_0+s)\rangle}{\langle V_k(t_0) V_k(t_0)\rangle}, \tag{3.7}$$

where $\boldsymbol{V}$ denotes fluctuations in particle velocity (or peculiar velocity) about the mean velocity computed by PR–DNS and s is the separation in time. The angular brackets $\langle\cdots\rangle$ in (3.7) denote an average over all particle configurations and velocities. The integral time scale for the autocorrelation function is

$$T_L = \int_0^\infty \rho(s)\,\mathrm{d}s. \tag{3.8}$$

If a stochastic process obeys the Langevin equation with an integral time scale of T_L, then its autocorrelation function should decay exponentially (Gardiner 1985), i.e. $\rho(s) = \mathrm{e}^{-s/T_L}$. The velocity autocorrelation function computed by PR–DNS of freely evolving gas–solid suspensions and the exponential decay predicted by the Langevin model are compared in figure 3. The good agreement of the decay of the velocity autocorrelation function obtained from PR–DNS with the exponential decay indicates that the use of the Langevin model is appropriate. In addition to the velocity autocorrelation function, we have also computed the time scale of decay of the autocorrelation of neighbour particles' contribution to the total fluctuating force

and compared it with the mean time between successive solid body collisions. Note that it is extremely difficult to isolate the contribution of the neighbour particles to the total fluctuating force obtained from PR–DNS. So we computed the neighbour particle contribution to the total fluctuating force indirectly as $(m\,\mathrm{d}\boldsymbol{V} + \boldsymbol{\gamma}\cdot\boldsymbol{V}\,\mathrm{d}t)$ in (2.1). Note that $m\,\mathrm{d}\boldsymbol{V}$ represents the total fluctuating force experienced by a particle, which is computed directly from PR–DNS. We found that for the highest Stokes number simulated ($St_m = 171$), there were only ∼2–3 collisions within the time scale of decay of the autocorrelation. For lower Stokes numbers, the number of collisions decreased to around 1 per fluid time scale. Note that the collisional time scale we used is valid for ballistic collisions, whereas in reality the presence of fluid could increase the time between collisions. From the decay of the velocity autocorrelation function as well as from the comparison of time scales we conclude that the neighbour particle effects can be modelled reasonably well by a stochastic Wiener process (Langevin model).

3.3. *Anisotropy in fluid and solid phases*

Although fluid motions even in homogeneous gas–solid flows are anisotropic in general, it is found that under the conditions considered in this work they still result in a nearly isotropic (particle) granular temperature. Consequently, we focus here on the simpler isotropic Langevin model for the particle velocity increment, since the already complex derivations of the transport coefficients would be even more involved for the more general anisotropic Langevin model. Therefore, although the quantities $\boldsymbol{\gamma}$ and $\boldsymbol{B}$ in (2.1) are given as tensors in the most general case, as a first approximation we take $\gamma_{ij} = \gamma\,\delta_{ij}$ and $B_{ij} = B\delta_{ij}$ to obtain a distribution function which is isotropic in velocity space for the homogeneous flow, and in addition provide analytical expressions for all the transport coefficients and the collisional cooling rate. We verify this assumption of isotropy by computing the state of anisotropy of the particle-phase Reynolds stress (RS), defined as the average $\langle V_i V_j\rangle$, from PR–DNS. The invariants of the deviatoric part of the normalized particle-phase RS, ξ_{RS} and η_{RS}, are plotted on the Lumley plane (Lumley & Newman 1977) to characterize the state of anisotropy. In the three-dimensional case, the deviatoric part of the normalized particle-phase RS is defined by

$$b_{ij} = \frac{\langle V_i V_j\rangle}{\langle V_k V_k\rangle} - \frac{1}{3}\delta_{ij}, \tag{3.9}$$

and the invariants are defined following Lumley & Newman (1977) as $6\eta_{RS}^2 = b_{ij}b_{ij}$ and $6\xi_{RS}^3 = b_{ij}b_{jk}b_{ki}$. The state of anisotropy of the particle-phase RS is studied by plotting η_{RS} versus ξ_{RS}. The origin of this plane denotes an isotropic state, while the point $(1/3, 1/3)$ denotes a one-component axisymmetric state of the particle-phase RS. The evolution of the invariants obtained from PR–DNS for $\phi = 0.35$, $\rho_s/\rho_g = 1000$ and two different Reynolds numbers ($Re_m = 1.0$ and $Re_m = 0.5$) is plotted in figure 4. The results show that the state of anisotropy in the solid phase is small for the range of physical parameters considered in this work, and hence the assumption of isotropic coefficients is justified. The results also indicate that the effect of collisions isotropizes the anisotropy introduced by fluid-dynamic interactions in the particle-phase RS.

This mechanism can be understood by analysing the evolution equation of the normalized deviatoric part of the particle-phase RS b_{ij} for a statistically homogeneous suspension, which is given by

$$\frac{\mathrm{d}b_{ij}}{\mathrm{d}t} = \frac{\Phi_{kk}}{3T}(b_{ij}^{\Phi} - b_{ij}) - \frac{b_{ij}}{\tau_{coll}}, \tag{3.10}$$

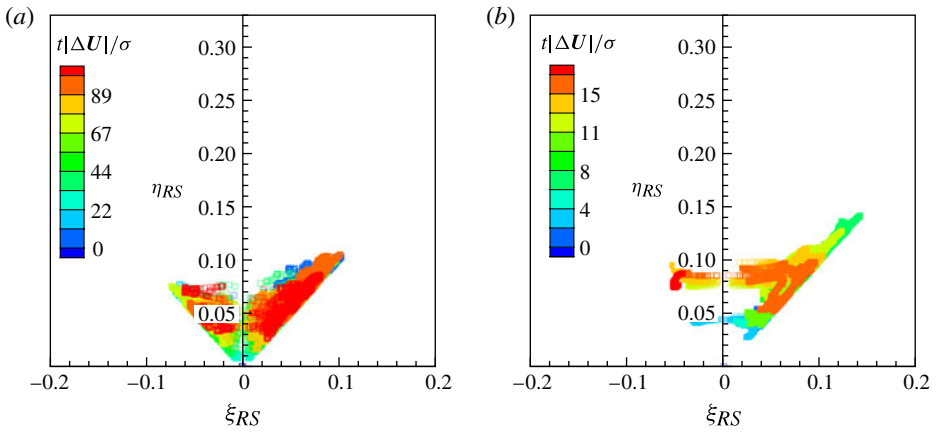

FIGURE 4. (Colour online) Evolution of the invariants of the deviatoric part of the normalized particle-phase RS in time. Dark (blue in colour online) symbols denote earlier time and light (red in colour online) symbols denote later time. These results are obtained from PR–DNS of freely evolving suspensions corresponding to a solid volume fraction of 0.35 and solid-to-fluid density ratio of 1000 for mean-flow Reynolds numbers (*a*) 1.0 and (*b*) 0.5.

where $\Phi_{kk} = \langle A_k'' V_k \rangle$ is the rate of change of particle granular temperature T, b_{ij}^{Φ} is the normalized deviatoric part of the acceleration–velocity covariance tensor $\langle A_i'' V_j \rangle + \langle A_j'' V_i \rangle$ and τ_{coll} is the collisional time scale. Here the A_j'' denote fluctuations in particle acceleration. When the suspension reaches a statistically stationary state, the rate of change of granular temperature is zero, i.e. $\Phi_{kk} = 0$, and hence the particle-phase RS returns to isotropy due to collisions. It is also worthwhile to note that this assumption is consistent for a homogeneous system, since the homogeneous (zeroth-order) solution to the kinetic equation (1.2) will be isotropic as no spatial gradients exist for a homogeneous system. Note that if the acceleration–velocity covariance tensor $\langle A_i'' V_j \rangle + \langle A_j'' V_i \rangle$ is decomposed into a source $S_{ij,h}$ and sink term $\Gamma_{ij,h}$ as in Koch (1990) and Koch & Sangani (1999), the source term in the particle-phase RS can be anisotropic in general. However, based on the low level of anisotropy in the particle velocity covariance, we conclude that an isotropic source term is a reasonable first approximation for the regime we are interested in. The description of the general case for $\boldsymbol{\gamma}$ and $\boldsymbol{B}$ is an interesting problem to be addressed in the future.

3.4. *Low Knudsen number*

The final assumption made in this work is related to the Chapman–Enskog expansion (see § 5 for further details), which is essentially a perturbation method about a small Knudsen number. The Knudsen number Kn is defined as the ratio of the mean free path of the particles to a length scale that characterizes the distance over which gradients in the hydrodynamic variables occur. The mean free path is a function of the solid volume fraction only, while the length scale associated with the gradients depends on the specific gas–solid flow system. Since the results in this work are applicable to any geometry and flow situation, assessment of this low-Kn assumption is not possible *a priori*.

4. Kinetic equation for gas–solid flows

We consider a suspension of solid particles of mass m and diameter σ immersed in a gas. Under rapid flow conditions, particles are usually modelled as a gas of

inelastic hard spheres. In the simplest model, the spheres are completely smooth so that the inelasticity of collisions is characterized by a (constant) coefficient of normal restitution $0 < \alpha \leqslant 1$. As described in § 2, the influence of the gas phase on particles is accomplished by the inclusion of three new quantities (see (2.1)) in the instantaneous particle force: β, γ and B.

Under the above conditions and in the presence of the gravitational force $m\boldsymbol{g}$, the Enskog kinetic equation (Brey, Dufty & Santos 1997; Brilliantov & Pöschel 2004) for the one-particle velocity distribution function $f(\boldsymbol{r}, \boldsymbol{v}, t)$ of grains reads

$$\partial_t f + \boldsymbol{v}\cdot\nabla f - \frac{\beta}{m}\Delta\boldsymbol{U}\cdot\frac{\partial f}{\partial \boldsymbol{V}} - \frac{\gamma}{m}\frac{\partial}{\partial \boldsymbol{V}}\cdot\boldsymbol{V}f - \frac{1}{2}\xi\frac{\partial^2}{\partial V^2}f + \boldsymbol{g}\cdot\frac{\partial f}{\partial \boldsymbol{V}} = J_E[\boldsymbol{r}, \boldsymbol{v}|f, f], \quad (4.1)$$

where

$$\begin{aligned} J_E[\boldsymbol{r}, \boldsymbol{v}_1|f, f] = \sigma^{d-1}\int \mathrm{d}\boldsymbol{v}_2 \int \mathrm{d}\,\widehat{\boldsymbol{\sigma}}\,\Theta(\widehat{\boldsymbol{\sigma}}\cdot\boldsymbol{g}_{12})(\widehat{\boldsymbol{\sigma}}\cdot\boldsymbol{g}_{12}) \\ \times[\alpha^{-2}\chi(\boldsymbol{r}, \boldsymbol{r}-\boldsymbol{\sigma})f(\boldsymbol{r}, \boldsymbol{v}_1'; t)f(\boldsymbol{r}-\boldsymbol{\sigma}, \boldsymbol{v}_2'; t) \\ - \chi(\boldsymbol{r}, \boldsymbol{r}+\boldsymbol{\sigma})f(\boldsymbol{r}, \boldsymbol{v}_1; t)f(\boldsymbol{r}+\boldsymbol{\sigma}, \boldsymbol{v}_2; t)] \end{aligned} \quad (4.2)$$

is the Enskog collision operator. Here, d is the dimensionality of the system ($d = 2$ for disks and $d = 3$ for spheres), $\boldsymbol{\sigma} = \sigma\widehat{\boldsymbol{\sigma}}$, $\widehat{\boldsymbol{\sigma}}$ being a unit vector pointing in the direction from the centre of particle 1 to the centre of particle 2, σ is the particle diameter, Θ is the Heaviside step function, $\boldsymbol{g}_{12} = \boldsymbol{v}_1 - \boldsymbol{v}_2$ and $\chi[\boldsymbol{r}, \boldsymbol{r}+\boldsymbol{\sigma}|\{n(t)\}]$ is the equilibrium pair correlation function at contact as a functional of the non-equilibrium density field $n(\boldsymbol{r}, t)$ defined by

$$n(\boldsymbol{r}, t) = \int \mathrm{d}\boldsymbol{v}\, f(\boldsymbol{r}, \boldsymbol{v}, t). \quad (4.3)$$

For the case of spheres ($d = 3$) considered in this work, the Carnahan–Starling approximation (Carnahan & Starling 1969) for χ is given by

$$\chi(\phi) = \frac{1 - \frac{1}{2}\phi}{(1-\phi)^3}. \quad (4.4)$$

The primes on the velocities in (4.2) denote the initial values $\{\boldsymbol{v}_1', \boldsymbol{v}_2'\}$ that lead to $\{\boldsymbol{v}_1, \boldsymbol{v}_2\}$ following a binary collision:

$$\boldsymbol{v}_1' = \boldsymbol{v}_1 - \tfrac{1}{2}\left(1+\alpha^{-1}\right)(\widehat{\boldsymbol{\sigma}}\cdot\boldsymbol{g}_{12})\widehat{\boldsymbol{\sigma}}, \quad \boldsymbol{v}_2' = \boldsymbol{v}_2 + \tfrac{1}{2}\left(1+\alpha^{-1}\right)(\widehat{\boldsymbol{\sigma}}\cdot\boldsymbol{g}_{12})\widehat{\boldsymbol{\sigma}}. \quad (4.5)$$

Moreover, in (4.1), $B^2 \equiv \xi$ and

$$\boldsymbol{U}(\boldsymbol{r}, t) = \frac{1}{n}\int \mathrm{d}\boldsymbol{v}\, \boldsymbol{v} f(\boldsymbol{r}, \boldsymbol{v}, t) \quad (4.6)$$

is the mean particle velocity. As said before, the scalar coefficients β, γ and ξ appearing in (4.1) are associated with the instantaneous gas–solid force. Recall that β appears in the mean portion of this drag force (first term on the right-hand side of (2.1)), and the terms γ and ξ are associated with the fluctuating solid velocity and particle momentum change caused by neighbour particles, respectively (Abbas, Climent & Simonin 2009).

The macroscopic balance equations for the system are obtained when one multiplies the Enskog equation (4.1) by $\{1, m\boldsymbol{V}, mV^2\}$ and integrates over velocity. After some

lengthy algebra one gets

$$D_t n + n\nabla\cdot\boldsymbol{U} = 0, \tag{4.7}$$

$$D_t \boldsymbol{U} + (mn)^{-1}\nabla\cdot\boldsymbol{P} = -\frac{\beta}{m}\Delta\boldsymbol{U} + \boldsymbol{g}, \tag{4.8}$$

$$D_t T + \frac{2}{\mathrm{d}n}(\nabla\cdot\boldsymbol{q} + \boldsymbol{P}:\nabla\boldsymbol{U}) = -\frac{2T}{m}\gamma + m\xi - \zeta T. \tag{4.9}$$

In the above equations, $D_t = \partial_t + \boldsymbol{U}\cdot\nabla$ is the material derivative and

$$T(\boldsymbol{r},t) = \frac{1}{\mathrm{d}n}\int \mathrm{d}\boldsymbol{v}\, mV^2 f(\boldsymbol{r},\boldsymbol{v},t) \tag{4.10}$$

is the granular temperature. This quantity is a measure of the mean square fluctuating particle velocity. The collisional cooling rate ζ is proportional to $1-\alpha^2$ and is due to dissipative collisions. The pressure tensor $\boldsymbol{P}(\boldsymbol{r},t)$ and the heat flux $\boldsymbol{q}(\boldsymbol{r},t)$ have both kinetic and collisional transfer contributions, i.e. $\boldsymbol{P} = \boldsymbol{P}^k + \boldsymbol{P}^c$ and $\boldsymbol{q} = \boldsymbol{q}^k + \boldsymbol{q}^c$. The kinetic, or streaming, contributions stem from the particles carrying momentum and granular energy with them as they travel from one part of the domain to another, while the collisional contributions arise from a transfer of momentum and granular energy between particles as they collide. The kinetic contributions $\boldsymbol{P}^k$ and $\boldsymbol{q}^k$ are given, respectively, by

$$\boldsymbol{P}^k(\boldsymbol{r},t) = \int \mathrm{d}\boldsymbol{v}\, m\boldsymbol{V}\boldsymbol{V} f(\boldsymbol{r},\boldsymbol{v},t), \quad \boldsymbol{q}^k(\boldsymbol{r},t) = \int \mathrm{d}\boldsymbol{v}\frac{m}{2}V^2\boldsymbol{V} f(\boldsymbol{r},\boldsymbol{v},t), \tag{4.11}$$

and the collisional transfer contributions are (Brey *et al.* 1997; Garzó & Dufty 1999)

$$\boldsymbol{P}^c(\boldsymbol{r},t) = \frac{1+\alpha}{4}m\sigma^d\int \mathrm{d}\boldsymbol{v}_1\int \mathrm{d}\boldsymbol{v}_2\int \mathrm{d}\widehat{\boldsymbol{\sigma}}\,\Theta(\widehat{\boldsymbol{\sigma}}\cdot\boldsymbol{g}_{12})(\widehat{\boldsymbol{\sigma}}\cdot\boldsymbol{g}_{12})^2\widehat{\boldsymbol{\sigma}}\,\widehat{\boldsymbol{\sigma}}$$
$$\times\int_0^1 \mathrm{d}x f^{(2)}[\boldsymbol{r}-x\boldsymbol{\sigma},\boldsymbol{r}+(1-x)\boldsymbol{\sigma},\boldsymbol{v}_1,\boldsymbol{v}_2;t], \tag{4.12}$$

$$\boldsymbol{q}^c(\boldsymbol{r},t) = \frac{1+\alpha}{4}m\sigma^d\int \mathrm{d}\boldsymbol{v}_1\int \mathrm{d}\boldsymbol{v}_2\int \mathrm{d}\widehat{\boldsymbol{\sigma}}\,\Theta(\widehat{\boldsymbol{\sigma}}\cdot\boldsymbol{g}_{12})(\widehat{\boldsymbol{\sigma}}\cdot\boldsymbol{g}_{12})^2(\boldsymbol{G}_{12}\cdot\widehat{\boldsymbol{\sigma}})\widehat{\boldsymbol{\sigma}}$$
$$\times\int_0^1 \mathrm{d}x f^{(2)}[\boldsymbol{r}-x\boldsymbol{\sigma},\boldsymbol{r}+(1-x)\boldsymbol{\sigma},\boldsymbol{v}_1,\boldsymbol{v}_2;t]. \tag{4.13}$$

Here, $\boldsymbol{G}_{12} = (\boldsymbol{V}_1+\boldsymbol{V}_2)/2$ is the velocity of centre of mass and

$$f^{(2)}(\boldsymbol{r}_1,\boldsymbol{r}_2,\boldsymbol{v}_1,\boldsymbol{v}_2,t) \equiv \chi(\boldsymbol{r}_1,\boldsymbol{r}_2|n(t))f(\boldsymbol{r}_1,\boldsymbol{v}_1,t)f(\boldsymbol{r}_2,\boldsymbol{v}_2,t). \tag{4.14}$$

Finally, the collisional cooling rate is given by

$$\zeta(\boldsymbol{r},t) = \frac{(1-\alpha^2)}{4\,\mathrm{d}nT}m\sigma^{d-1}\int \mathrm{d}\boldsymbol{v}_1\int \mathrm{d}\boldsymbol{v}_2$$
$$\times\int \mathrm{d}\widehat{\boldsymbol{\sigma}}\,\Theta(\widehat{\boldsymbol{\sigma}}\cdot\boldsymbol{g}_{12})(\widehat{\boldsymbol{\sigma}}\cdot\boldsymbol{g}_{12})^3 f^{(2)}(\boldsymbol{r},\boldsymbol{r}+\boldsymbol{\sigma},\boldsymbol{v}_1,\boldsymbol{v}_2;t). \tag{4.15}$$

For a statistically homogeneous suspension undergoing elastic collisions ($\alpha = 1$), $\zeta = 0$ and the granular energy equation (4.9) becomes

$$\frac{\mathrm{d}T}{\mathrm{d}t} = -\frac{2T}{m}\gamma + m\xi. \tag{4.16}$$

Comparing this equation with the granular energy equation given for spheres ($d = 3$) by Koch & Sangani (1999),

$$\frac{3}{2}\frac{\mathrm{d}T}{\mathrm{d}t} = -\Gamma_{vis} + S, \tag{4.17}$$

we see that there is a one-to-one correspondence between the coefficients γ and ξ and the dissipation Γ_{vis} and source S in Koch & Sangani (1999), respectively. Therefore, for Stokes flow we can use the existing analytical closure from Koch (1990) for solid volume fraction $\phi \leqslant 0.1$. For $\phi > 0.1$, Koch & Sangani (1999) used simulations based on multipole expansions to propose source and dissipation terms as a function of solid volume fraction. It must be noted that the correlation used for the drag coefficient does not include the effect of forces such as buoyancy, shear lift or spin lift. Accordingly, these coefficients depend on constant parameters (particle mass and diameter, gas viscosity) as well as the hydrodynamic (mean) variables (solids concentration, gas and solid velocities, and granular temperature); explicit dependences are given in § 8.

The macroscopic balance equations (4.7)–(4.9) are not entirely expressed in terms of the hydrodynamic fields due to the presence of the collisional cooling rate ζ, the pressure tensor $\boldsymbol{P}$ and the heat flux $\boldsymbol{q}$, which are given as functionals of the distribution function $f(\boldsymbol{r}, \boldsymbol{v}, t)$. However, if this distribution function can be expressed as functionals of the hydrodynamic fields, then the collisional cooling rate and the fluxes will also become functionals of the hydrodynamic fields through (4.11)–(4.13) and (4.15). Such expressions are called constitutive relations and are the link between the exact balance equations and a closed set of equations for the fields n, $\boldsymbol{U}$ and T. This hydrodynamic description can be derived by looking for a normal solution to the Enskog equation by means of the Chapman–Enskog (CE) method (Chapman & Cowling 1970) adapted to inelastic collisions, as detailed in § 5.

It is worthwhile to note that the macroscopic equations given in (4.7)–(4.9) differ from their granular (no gas phase) counterparts (Garzó & Dufty 1999) via the appearance of three additional terms arising from the presence of the gas phase, and more specifically the instantaneous drag force (equation (2.1)). The first of these contains β and appears in the momentum balance (equation (4.8)); this term represents the mean drag force between the two phases. The other two terms stemming from the gas phase appear in the granular energy balance (equation (4.9)); the term containing γ represents the sink due to viscous drag while the term containing ξ represents the source arising from the change in particle momentum due to neighbour particles. Similar effects of the gas phase on the constitutive expressions for the pressure tensor $\boldsymbol{P}$, the heat flux $\boldsymbol{q}$ and the collisional cooling rate ζ will be presented in §§ 6 and 7.

5. Chapman–Enskog solution

The CE method assumes the existence of a normal solution such that all space and time dependence of the distribution function occurs through the hydrodynamic fields

$$f(\boldsymbol{r}, \boldsymbol{v}, t) = f[\boldsymbol{v}|n(\boldsymbol{r}, t), T(\boldsymbol{r}, t), \boldsymbol{U}(\boldsymbol{r}, t)]. \tag{5.1}$$

The notation on the right-hand side indicates a functional dependence on the density, temperature and flow velocity. For small spatial variations (i.e. low Knudsen numbers), this functional dependence can be made local in space through an expansion in gradients of the hydrodynamic fields. To generate it, f is written as a series expansion in a formal parameter ϵ measuring the non-uniformity of the system,

$$f = f^{(0)} + \epsilon f^{(1)} + \epsilon^2 f^{(2)} + \cdots, \tag{5.2}$$

where each factor of ϵ means an implicit gradient of a hydrodynamic field. The uniformity parameter ϵ is related to the Knudsen number Kn defined as the ratio of the mean free path of the particles to a length scale that characterizes the distance over which gradients in the hydrodynamic variables occur. Note that while the strength of the gradients can be controlled by the initial or boundary conditions in the case of elastic collisions, the problem is more complicated for granular fluids since in some cases, e.g. steady states such as simple shear flow (Goldhirsch 2003; Santos, Garzó & Dufty 2004), there is an intrinsic relation between dissipation and some hydrodynamic gradient. In these situations the Navier–Stokes approximation (first-order in the expansion) only applies for nearly elastic systems (Goldhirsch 2003). Here, however, we consider situations where the spatial gradients are sufficiently small (low Knudsen number) (Hrenya, Galvin & Wildman 2008). Moreover, in ordering the different level of approximations in the kinetic equation, one has to characterize the magnitude of the external forces relative to the gradients as well. The scaling of the forces depends on the conditions of interest. Here, we assume that the external forces (gravity and drag forces) do not induce any flux in the system and only modify the form of the transport coefficients. As a consequence, g, β, γ and ξ are taken to be of zeroth order in gradients.

According to the expansion (5.2) for the distribution function, the Enskog collision operator and time derivative are also given in the representations

$$J_E = J_E^{(0)} + \epsilon J_E^{(1)} + \cdots, \quad \partial_t = \partial_t^{(0)} + \epsilon \partial_t^{(1)} + \cdots. \tag{5.3}$$

The coefficients in the time derivative expansion are identified by a representation of the fluxes and the collisional cooling rate in the macroscopic balance equations as a similar series through their definitions as functionals of f. This is the usual CE method (Chapman & Cowling 1970; Garzó & Santos 2003) for solving kinetic equations. The main difference here with respect to previous works (Brey *et al.* 1998; Garzó & Dufty 1999) is that the reference state $f^{(0)}$ has a time dependence associated with the fluid phase terms γ and ξ apart from the one associated with the collisional cooling rate that is not proportional to the gradients. As a consequence, terms from the time derivative $\partial_t^{(0)}$ are not zero as expected. In addition, given that collisional dissipation and gradients are uncoupled, the different approximations $f^{(k)}$ are nonlinear functions of α, regardless of the applicability of the corresponding hydrodynamic equations truncated at that order.

To summarize, the Chapman–Enskog expansion is carried out up to first order (Navier–Stokes order), resulting in constitutive equations which are proportional to the first-order spatial derivatives in the hydrodynamic fields. This first-order expansion is strictly valid for small Knudsen number Kn. Because the length scale for variations of the hydrodynamic fields depends on the local flow field, the assumption of small Kn (also known as the 'small gradient' assumption) may be valid for some flow geometries and invalid for others. Since our results are presented below in a general form (prior to the application for any specific flow geometry), assessment of this low-Knudsen assumption is not possible *a priori*. Nonetheless, it is worth noting that for ordinary fluids, the Navier–Stokes hydrodynamic equations work well beyond their range of validity expected from a strict application of their assumptions. The same has also been found to be true for granular fluids; namely, the range of applicability of the Navier–Stokes description, based on comparisons with experimental data, is often much wider than expected (Rericha *et al.* 2002; Wildman *et al.* 2008).

6. Local homogeneous state: zeroth-order solution

To zeroth order in ϵ, the Enskog equation (4.1) becomes

$$\partial_t^{(0)} f^{(0)} - \frac{\beta}{m}\Delta \boldsymbol{U}\cdot\frac{\partial f^{(0)}}{\partial \boldsymbol{V}} - \frac{\gamma}{m}\frac{\partial}{\partial \boldsymbol{V}}\cdot \boldsymbol{V} f^{(0)} - \frac{1}{2}\xi\frac{\partial^2}{\partial V^2} f^{(0)} + \boldsymbol{g}\cdot\frac{\partial f^{(0)}}{\partial \boldsymbol{V}} = J_E^{(0)}[f^{(0)}, f^{(0)}], \quad (6.1)$$

where

$$J_E^{(0)}\left[f^{(0)}, f^{(0)}\right] \equiv \chi\sigma^{d-1}\int \mathrm{d}\boldsymbol{v}_2 \int \mathrm{d}\,\widehat{\boldsymbol{\sigma}}\,\Theta(\widehat{\boldsymbol{\sigma}}\cdot\boldsymbol{g}_{12})(\widehat{\boldsymbol{\sigma}}\cdot\boldsymbol{g}_{12}) \times \left[\alpha^{-2} f^{(0)}(v_1') f^{(0)}(v_2') - f^{(0)}(v_1) f^{(0)}(v_2)\right]. \quad (6.2)$$

Here, $\chi \equiv \chi[\boldsymbol{r}, \boldsymbol{r}+\boldsymbol{\sigma}|n(t)]|_{n=n(t)}$ is the pair functional evaluated with all density fields at the local point $\boldsymbol{r}$. The collision operator (6.2) can be recognized as the Boltzmann operator for inelastic collisions multiplied by the factor χ. Note that in (6.1) all spatial gradients are neglected at this lowest order. Moreover, as discussed before, upon writing (6.1) it has been assumed that the gravity field and the external parameters accounting for the effects of the gas phase are taken to be of zeroth order in spatial gradients. The macroscopic balance equations at this order are

$$\partial_t^{(0)} n = 0, \quad \partial_t^{(0)}\boldsymbol{U} = -\frac{\beta}{m}\Delta\boldsymbol{U} + \boldsymbol{g}, \quad (6.3)$$

$$\partial_t^{(0)} T = -\frac{2T}{m}\gamma + m\xi - \zeta^{(0)} T, \quad (6.4)$$

where $\zeta^{(0)}$ is determined by (4.15) to zeroth order, namely, by using the distribution $f^{(0)}$. Since $f^{(0)}$ qualifies as a normal solution, then

$$\partial_t^{(0)} f^{(0)} = \frac{\partial f^{(0)}}{\partial n}\partial_t^{(0)} n + \frac{\partial f^{(0)}}{\partial U_i}\partial_t^{(0)} U_i + \frac{\partial f^{(0)}}{\partial T}\partial_t^{(0)} T = \left(\frac{\beta}{m}\Delta\boldsymbol{U} - \boldsymbol{g}\right)\cdot\frac{\partial f^{(0)}}{\partial \boldsymbol{V}} - \left(\frac{2\gamma}{m} - \frac{m}{T}\xi + \zeta^{(0)}\right) T\frac{\partial f^{(0)}}{\partial T}, \quad (6.5)$$

where in the last step we have taken into account that $f^{(0)}$ depends on $\boldsymbol{U}$ through its dependence on $\boldsymbol{V}$. Substitution of (6.5) into (6.1) yields

$$-\left(\frac{2}{m}\gamma - \frac{m}{T}\xi + \zeta^{(0)}\right) T\frac{\partial f^{(0)}}{\partial T} - \frac{\gamma}{m}\frac{\partial}{\partial \boldsymbol{V}}\cdot\boldsymbol{V} f^{(0)} - \frac{1}{2}\xi\frac{\partial^2}{\partial V^2} f^{(0)} = J_E^{(0)}[f^{(0)}, f^{(0)}]. \quad (6.6)$$

Since the solution to (6.6) is isotropic in $\boldsymbol{V}$, dimensional analysis requires that $f^{(0)}$ has the scaled form

$$f^{(0)}(\boldsymbol{V}) = n v_0^{-d}\Psi\left(\frac{V}{v_0}\right), \quad (6.7)$$

where Ψ is an unknown function of $\boldsymbol{V}/v_0$, where $v_0 = \sqrt{2T/m}$ is the thermal speed. Therefore, according to (6.7), the temperature dependence of $f^{(0)}$ can occur only through v_0 and the dimensionless velocity V/v_0 so that

$$T\frac{\partial f^{(0)}}{\partial T} = -\frac{1}{2}\frac{\partial}{\partial \boldsymbol{V}}\cdot\boldsymbol{V} f^{(0)}. \quad (6.8)$$

Taking into account (6.7) and (6.8), the Enskog equation (6.6) for the zeroth-order distribution function finally becomes

$$\frac{1}{2}\left(\zeta^{(0)}-\frac{m\xi}{T}\right)\frac{\partial}{\partial \boldsymbol{V}}\cdot \boldsymbol{V}f^{(0)}-\frac{1}{2}\xi\frac{\partial^2}{\partial V^2}f^{(0)}=J_E^{(0)}[f^{(0)},f^{(0)}]. \tag{6.9}$$

Note that (6.9) is independent of the parameters β and γ. In fact, when $\xi=0$, one recovers the kinetic equation defining the homogeneous cooling state (HCS), whose solution has been previously worked out by several authors (van Noije & Ernst 1998; Montanero & Santos 2000; Pöschel & Brilliantov 2006; Santos & Montanero 2009).

In terms of the (scaled) distribution Ψ, (6.9) can be rewritten as

$$\frac{1}{2}\left(\zeta^*-\xi^*\right)\frac{\partial}{\partial \boldsymbol{c}}\cdot \boldsymbol{c}\Psi-\frac{1}{4}\xi^*\frac{\partial^2}{\partial c^2}\Psi=J_E^*[\Psi,\Psi], \tag{6.10}$$

where $\boldsymbol{c}=\boldsymbol{V}/v_0$,

$$\zeta^*=\frac{\ell\zeta^{(0)}}{v_0},\quad \xi^*=\frac{m\xi\ell}{Tv_0},\quad J_E^*=\frac{\ell}{n}v_0^{d-1}J_E^{(0)}, \tag{6.11}$$

and $\ell=1/(n\sigma^{d-1})$ is the (local) mean free path for hard spheres. It must be noted that upon deriving (6.7)–(6.10) we have assumed that the reduced parameters γ^* and ξ^* do not depend on the granular temperature. This assumption will be confirmed later when we express γ^* and ξ^* in terms of the Reynolds numbers (see (8.9) and (8.10) for γ^* and ξ^*, respectively).

In the case of elastic particles ($\alpha=1$), $\zeta^*=0$ and the solution of (6.10) is a Maxwellian distribution Koch (1990):

$$\Psi(\boldsymbol{c})=\pi^{-d/2}\mathrm{e}^{-c^2}. \tag{6.12}$$

However, if the particles collide inelastically ($\alpha<1$), the exact form of $\Psi(\boldsymbol{c})$ is not known, even in the dry granular case ($\xi^*=0$). However, a very good approximation can be obtained from an expansion in Sonine polynomials (van Noije & Ernst 1998). In particular, since the distribution function is isotropic, the zeroth-order pressure tensor and heat flux are found from (4.11)–(4.13) to be

$$P_{ij}^{(0)}=p\,\delta_{ij},\quad \boldsymbol{q}^{(0)}=\boldsymbol{0}, \tag{6.13}$$

where the hydrostatic pressure p is

$$p=nT[1+2^{d-2}(1+\alpha)\chi\phi], \tag{6.14}$$

where

$$\phi=\frac{\pi^{d/2}}{2^{d-1}d\Gamma\left(\frac{d}{2}\right)}n\sigma^d \tag{6.15}$$

is the solid volume fraction. Note that the presence of the gas phase does not enter the constitutive relation for pressure.

The deviation of $\Psi(c)$ from its Maxwellian form is measured through the kurtosis or fourth-cumulant (van Noije & Ernst 1998)

$$a_2=\frac{4}{d(d+2)}\langle c^4\rangle-1, \tag{6.16}$$

where

$$\langle c^k \rangle = \int \mathrm{d}\boldsymbol{c}\, c^k \Psi(c). \tag{6.17}$$

In order to determine a_2, we multiply both sides of (6.10) by c^4 and integrate over velocity. The result is

$$\frac{d(d+2)}{2}\left[\zeta^*(1+a_2) - \xi^* a_2\right] = \mu_4, \tag{6.18}$$

where

$$\mu_k = -\int \mathrm{d}\boldsymbol{c}\, c^k J_E^*[\Psi, \Psi]. \tag{6.19}$$

Upon writing (6.18) use has been made of the partial result

$$\int \mathrm{d}\boldsymbol{c}\, c^p \frac{\partial^2 \Psi}{\partial c^2} = p(p+d-2)\langle c^{p-2}\rangle \tag{6.20}$$

with $p = 4$ and $\langle c^2 \rangle = d/2$.

Equation (6.18) is still exact. To get an approximate expression for the quantities $\zeta^* = (2/d)\mu_2$ and μ_4, we consider the first Sonine approximation for Ψ; then we insert this expansion into (6.19) and neglect terms nonlinear in a_2. The results are

$$\mu_2 \to \mu_2^{(0)} + \mu_2^{(1)} a_2, \quad \mu_4 \to \mu_4^{(0)} + \mu_4^{(1)} a_2, \tag{6.21}$$

where (van Noije & Ernst 1998)

$$\mu_2^{(0)} = \frac{\pi^{(d-1)/2}}{\sqrt{2}\Gamma\left(\frac{d}{2}\right)} \chi(1-\alpha^2), \quad \mu_2^{(1)} = \frac{3}{16}\mu_2^{(0)}, \tag{6.22}$$

$$\mu_4^{(0)} = \left(d + \frac{3}{2} + \alpha^2\right)\mu_2^{(0)}, \tag{6.23}$$

$$\mu_4^{(1)} = \left[\frac{3}{32}(10d + 39 + 10\alpha^2) + \frac{d-1}{1-\alpha}\right]\mu_2^{(0)}, \tag{6.24}$$

and in (6.22), Γ refers to the Gamma function. With the use of the approximations (6.21) and retaining only linear terms in a_2, the solution to (6.18) is

$$a_2 = -\frac{\mu_4^{(0)} - (d+2)\mu_2^{(0)}}{\mu_4^{(1)} - (d+2)\left(\frac{19}{16}\mu_2^{(0)} - \frac{d}{2}\xi^*\right)}. \tag{6.25}$$

In terms of a_2, the zeroth-order expression $\zeta^{(0)}$ for the collisional cooling rate can be written as

$$\zeta^{(0)} = \frac{2}{d}\frac{\pi^{(d-1)/2}}{\Gamma\left(\frac{d}{2}\right)}(1-\alpha^2)\chi\left(1 + \frac{3}{16}a_2\right) n\sigma^{d-1}\sqrt{\frac{T}{m}}. \tag{6.26}$$

Note that the effects of the interstitial gas on the zeroth-order collisional cooling rate $\zeta^{(0)}$ is only through the dependence of the kurtosis a_2 on ξ^* (equation (6.25)).

7. First-order solution: Navier–Stokes transport coefficients

The analysis to first order in the expansion parameter is similar to that worked out by Garzó & Dufty (1999) and Lutsko (2005) in the dry granular case. We only display here the final expressions for the fluxes and the collisional cooling rate, with some details being given in appendices A and B. The form of the first-order velocity distribution function $f^{(1)}$ is given by

$$f^{(1)} = \boldsymbol{\mathcal{A}}(\boldsymbol{V}) \cdot \boldsymbol{\nabla} \ln T + \boldsymbol{\mathcal{B}}(\boldsymbol{V}) \cdot \boldsymbol{\nabla} \ln n + \mathscr{C}_{ij}(\boldsymbol{V}) \frac{1}{2} \left(\partial_i U_j + \partial_j U_i - \frac{2}{d} \delta_{ij} \boldsymbol{\nabla} \cdot \boldsymbol{U} \right) + \mathscr{D}(\boldsymbol{V}) \boldsymbol{\nabla} \cdot \boldsymbol{U}, \tag{7.1}$$

where the quantities $\boldsymbol{\mathcal{A}}(\boldsymbol{V})$, $\boldsymbol{\mathcal{B}}(\boldsymbol{V})$, $\mathscr{C}_{ij}(\boldsymbol{V})$ and $\mathscr{D}(\boldsymbol{V})$ are the solutions of the linear integral equations (A 18)–(A 21), respectively. With the distribution function $f^{(1)}$ determined by (7.1), the pressure tensor, the heat flux and the collisional cooling rate can be calculated to first order in the spatial gradients. It is worthwhile to note that the spatial dependence of ξ with respect to $|\Delta \boldsymbol{U}|$ (see (8.2) below) has been neglected in these calculations (unlike the spatial dependence with respect to the density n and the granular temperature T). This assumption is due to the applications which motivate this work. Namely, in circulating fluidized beds (CFBs), the solid concentration and granular temperature vary considerably in space, whereas the relative velocity $\Delta \boldsymbol{U}$ remains relatively constant ($\sim$ terminal velocity of single particle). Accordingly, $\Delta \boldsymbol{U}$ is treated as a constant here, which also has the benefit of greatly simplifying the calculations. It is also important to remark that our results have been derived systematically from the inelastic Enskog equation by the CE procedure, and consequently there is no *a priori* limitation on the degree of inelasticity. Thus, the results apply to a wide range of values of the coefficient of restitution. Moreover, since the transport coefficients and the collisional cooling rate are given in terms of the solutions of the coupled linear integral equations (A 18)–(A 21), for practical purposes these integral equations have been solved by truncated expansions in Sonine polynomials.

The forms of the collisional contributions to the momentum and heat fluxes are exactly the same as those obtained in the absence of the gas phase (Garzó & Dufty 1999; Lutsko 2005), except that a_2 depends on ξ^*. Thus, we will focus our attention on evaluation of the kinetic parts of the transport coefficients and the collisional cooling rate. Some technical details of this calculation are provided in appendix B. Let us consider each flux separately.

7.1. *Pressure tensor*

To first order, the pressure tensor is given by

$$P_{ij}^{(1)} = -\eta \left(\partial_i U_j + \partial_j U_i - \frac{2}{d} \delta_{ij} \boldsymbol{\nabla} \cdot \boldsymbol{U} \right) - \lambda \delta_{ij} \boldsymbol{\nabla} \cdot \boldsymbol{U}, \tag{7.2}$$

where η is the shear viscosity and λ is the bulk viscosity. While the shear viscosity has kinetic and collisional contributions, the bulk viscosity has only a collisional contribution. The shear viscosity is

$$\eta = \eta_k + \eta_c. \tag{7.3}$$

The collisional contribution η_c to the shear viscosity η is given by (Garzó & Dufty 1999; Lutsko 2005)

$$\eta_c = \frac{2^{d-1}}{d+2}\phi\chi(1+\alpha)\eta_k + \frac{d}{d+2}\lambda, \tag{7.4}$$

and the bulk viscosity is

$$\lambda = \frac{2^{2d+1}}{\pi(d+2)}\phi^2\chi(1+\alpha)\left(1-\frac{a_2}{16}\right)\eta_0. \tag{7.5}$$

Here,

$$\eta_0 = \frac{d+2}{8}\frac{\Gamma\left(\frac{d}{2}\right)}{\pi^{(d-1)/2}}\sigma^{1-d}\sqrt{mT} \tag{7.6}$$

is the low-density value of the shear viscosity in the elastic limit. The kinetic part η_k of the shear viscosity is

$$\eta_k = \frac{nT}{\nu_\eta - \frac{1}{2}\left(\zeta^{(0)} - \frac{m}{T}\xi - \frac{2}{m}\gamma\right)}\left[1 - \frac{2^{d-2}}{d+2}(1+\alpha)(1-3\alpha)\phi\chi\right], \tag{7.7}$$

where the collision frequency ν_η is (Garzó, Santos & Montanero 2007*c*)

$$\nu_\eta = \frac{3\nu_0}{4d}\chi\left(1-\alpha+\frac{2}{3}d\right)(1+\alpha)\left(1+\frac{7}{16}a_2\right). \tag{7.8}$$

Here, $\nu_0 = nT/\eta_0$. The shear viscosity can finally be written as

$$\eta = \eta_k\left[1 + \frac{2^{d-1}}{d+2}\phi\chi(1+\alpha)\right] + \frac{d}{d+2}\lambda. \tag{7.9}$$

Thus, in addition to the presence of a_2 (which depends on ξ) in (7.5) for the bulk viscosity, gas-phase effects appear explicitly in the kinetic part η_k of the shear viscosity via the appearance of γ and ξ in (7.7) and implicitly via the appearance of ν_η, which also depends on a_2 (see (7.8)).

7.2. *Heat flux*

The constitutive form for the heat flux in the Navier–Stokes approximation is

$$\boldsymbol{q}^{(1)} = -\kappa\boldsymbol{\nabla}T - \mu\boldsymbol{\nabla}n, \tag{7.10}$$

where κ is the thermal conductivity and μ is the Dufour coefficient, which is not present in the granular case (no gas phase) when particles collide elastically ($\alpha = 1$).

The thermal conductivity κ is given by

$$\kappa = \kappa_k + \kappa_c. \tag{7.11}$$

The collisional contribution κ_c to the thermal conductivity κ is (Garzó & Dufty 1999; Lutsko 2005)

$$\kappa_c = 3\frac{2^{d-2}}{d+2}\phi\chi(1+\alpha)\kappa_k + \frac{2^{2d+1}(d-1)}{(d+2)^2\pi}\phi^2\chi(1+\alpha)\left(1+\frac{7}{16}a_2\right)\kappa_0, \tag{7.12}$$

where

$$\kappa_0 = \frac{d(d+2)}{2(d-1)}\frac{\eta_0}{m} \tag{7.13}$$

is the thermal conductivity coefficient of an elastic dilute gas. The expression of the kinetic part κ_k is

$$\kappa_k = \frac{d-1}{d}\kappa_0\nu_0\left(\nu_\kappa + \frac{1}{2}\frac{m\xi}{T} - 2\zeta^{(0)} - \frac{2T}{m}\gamma_T + m\xi_T\right)^{-1} \times \left\{1 + 2a_2 + 3\frac{2^{d-3}}{d+2}\phi\chi\,(1+\alpha)^2\left[2\alpha - 1 + a_2(1+\alpha)\right]\right\}, \tag{7.14}$$

where

$$\gamma_T \equiv \frac{\partial\gamma}{\partial T}, \quad \xi_T \equiv \frac{\partial\xi}{\partial T}, \tag{7.15}$$

and the collision frequency ν_κ is given by (Garzó *et al.* 2007*c*)

$$\nu_\kappa = \nu_0\frac{1+\alpha}{d}\chi\left[\frac{d-1}{2} + \frac{3}{16}(d+8)(1-\alpha) + \frac{296 + 217d - 3(160+11d)\alpha}{256}a_2\right]. \tag{7.16}$$

The (combined) thermal conductivity κ can finally be written as

$$\kappa = \kappa_k\left[1 + 3\frac{2^{d-2}}{d+2}\phi\chi(1+\alpha)\right] + \frac{2^{2d+1}(d-1)}{(d+2)^2\pi}\phi^2\chi(1+\alpha)\left(1 + \frac{7}{16}a_2\right)\kappa_0. \tag{7.17}$$

The Dufour coefficient is given by

$$\mu = \mu_k + \mu_c, \tag{7.18}$$

where the expression for the collisional contribution μ_c is (Garzó & Dufty 1999; Lutsko 2005)

$$\mu_c = 3\frac{2^{d-2}}{d+2}\phi\chi(1+\alpha)\mu_k. \tag{7.19}$$

The kinetic contribution μ_k is given by

$$\mu_k = \frac{\kappa_0\nu_0 T}{n}\left[\nu_\kappa - \frac{3}{2}\left(\zeta^{(0)} - \frac{m\xi}{T}\right)\right]^{-1}\left\{\frac{\kappa_k}{\kappa_0\nu_0}\left[\frac{2n}{m}\gamma_n - \frac{\rho}{T}\xi_n + \zeta^{(0)}\left(1 + \phi\partial_\phi\ln\chi\right)\right] + \frac{d-1}{d}a_2 + 3\frac{2^{d-2}(d-1)}{d(d+2)}\phi\chi(1+\alpha)\left(1 + \frac{1}{2}\phi\partial_\phi\ln\chi\right) \times \left[\alpha(\alpha-1) + \frac{a_2}{6}(10 + 2d - 3\alpha + 3\alpha^2)\right]\right\}, \tag{7.20}$$

where

$$\gamma_n \equiv \frac{\partial\gamma}{\partial n}, \quad \xi_n \equiv \frac{\partial\xi}{\partial n}. \tag{7.21}$$

The (combined) Dufour coefficient μ can be written as

$$\mu = \mu_k \left[1 + 3\frac{2^{d-2}}{d+2}\phi\chi(1+\alpha) \right]. \tag{7.22}$$

In the granular case (no gas phase, and so $\beta = \gamma = \xi = 0$), the Dufour coefficient vanishes for elastic collisions ($\alpha = 1$). On the other hand, (7.22) shows that $\mu \neq 0$ when the gas phase is accounted for, even for elastic collisions. In this case ($\alpha = 1$), $a_2 = 0$ and the Dufour coefficient μ is given by (7.22) with

$$\mu_k = \frac{\kappa_k T}{n}\left(\nu_\kappa + \frac{3}{2}\frac{m\xi}{T}\right)^{-1}\left(\frac{2n}{m}\gamma_n - \frac{\rho}{T}\xi_n\right), \tag{7.23}$$

where κ_k is given by (7.14) with $\alpha = 1$, and $a_2 = \zeta^{(0)} = 0$.

Again, similar to the pressure tensor, gas-phase effects appear implicitly in the thermal conductivity and Dufour coefficients via the appearance of the cumulant a_2 (which depends on ξ) in (7.14), (7.17) and (7.20). Furthermore, such effects are explicit in the kinetic contributions to the thermal conductivity and the Dufour coefficient (see (7.14) and (7.20)) through the terms containing γ and ξ.

7.3. *Collisional cooling rate*

The collisional cooling rate ζ is given by

$$\zeta = \zeta^{(0)} + \zeta_U \boldsymbol{\nabla}\cdot\boldsymbol{U}, \tag{7.24}$$

where $\zeta^{(0)}$ is defined in (6.26). At first order in gradients, the proportionality constant ζ_U is a new transport coefficient for granular fluids. This coefficient is given by

$$\zeta_U = \zeta_{10} + \zeta_{11}, \tag{7.25}$$

where

$$\zeta_{10} = -3\frac{2^{d-2}}{d}\chi\phi(1-\alpha^2), \tag{7.26}$$

$$\zeta_{11} = \frac{27\,(d+2)^2\,2^{d-8}}{32d^3}\phi\chi^2(1-\alpha^2) \times \frac{\left(1+\frac{3a_2}{128}\right)\left[\frac{\omega}{2(d+2)} - (1+\alpha)\nu_0\left(\frac{1}{3}-\alpha\right)\frac{a_2}{2}\right]}{\nu_\gamma + \frac{\gamma}{m} + \frac{3m\xi}{2T} - \frac{3}{2}\zeta^{(0)}}. \tag{7.27}$$

In the above expression, the collision frequencies ω and ν_γ are given by (Garzó & Dufty 1999; Lutsko 2005)

$$\omega = (1+\alpha)\nu_0\left\{(1-\alpha^2)(5\alpha-1) - \frac{a_2}{6}\left[15\alpha^3 - 3\alpha^2 + 3(4d+15)\alpha - (20d+1)\right]\right\}, \tag{7.28}$$

$$\nu_\gamma = -\frac{1+\alpha}{192}\chi\nu_0\left[30\alpha^3 - 30\alpha^2 + (105+24d)\alpha - 56d - 73\right]. \tag{7.29}$$

The presence of the gas phase impacts ζ_{11} via the explicit appearance of γ and ξ (see (7.27)) as well as an implicit dependence via the cumulant a_2.

8. Results and discussion

8.1. *Drag model: low mean-flow Reynolds numbers*

The expressions derived in §§ 6 and 7 for the (reduced) transport coefficients and the collisional cooling rate depend on the coefficient of restitution α, the solid volume fraction ϕ along with the external parameters γ and ξ and their derivatives with respect to the density n and the granular temperature T. Thus, to show the explicit forms of η, λ, κ, μ and ζ_U, one has to provide relations for γ and ξ. As described in § 4, these quantities are derived from the Stokes flow closures for the source and dissipation of granular energy given by Koch (1990) and Koch & Sangani (1999). Recall that attention here is limited to low mean-flow Reynolds numbers in order to compare with previous analytical results (Koch 1990; Koch & Sangani 1999) and to assess the impact of the gas phase on the constitutive relations, the latter of which was neglected in the analytical treatment.

We consider here the physical case of hard spheres ($d = 3$). For the case of low mean-flow Reynolds numbers, the expressions of γ and ξ are given by

$$\gamma = \frac{m}{\tau} R_{diss}(\phi), \tag{8.1}$$

$$\xi = \frac{1}{6\sqrt{\pi}} \frac{\sigma\,|\Delta \boldsymbol{U}|^2}{\tau^2 \sqrt{\dfrac{T}{m}}} S^*(\phi), \tag{8.2}$$

where $\tau = m/(3\pi\mu_g\sigma)$ is the characteristic time scale over which the velocity of a particle of mass m and diameter σ relaxes due to viscous forces. Here, μ_g is the gas viscosity.

In the case of dilute suspensions ($0 \leqslant \phi \leqslant 0.1$), the expressions for the functions $R_{diss}(\phi)$ and $S^*(\phi)$ are (Koch 1990)

$$R_{diss}(\phi) = 1 + 3\sqrt{\frac{\phi}{2}}, \quad S^*(\phi) = 1. \tag{8.3}$$

For moderately dense suspensions ($0.1 \leqslant \phi \leqslant 0.4$), the functions $R_{diss}(\phi)$ and $S^*(\phi)$ can be well approximated by (Sangani *et al.* 1996; Koch & Sangani 1999)

$$R_{diss}(\phi) = 1 + 3\sqrt{\frac{\phi}{2}} + \frac{135}{64}\phi \ln\phi + 11.26\phi\left(1 - 5.1\phi + 16.57\phi^2 - 21.77\phi^3\right) - \phi\chi(\phi)\ln\epsilon_m, \tag{8.4}$$

$$S^*(\phi) = \frac{R_{drag}^2}{\chi(\phi)\left(1 + 3.5\sqrt{\phi} + 5.9\phi\right)}, \tag{8.5}$$

where the function R_{drag} is given by

$$R_{drag}(\phi) = \frac{1 + 3\sqrt{\dfrac{\phi}{2}} + \dfrac{135}{64}\phi\ln\phi + 17.14\phi}{1 + 0.681\phi - 8.48\phi^2 + 8.16\phi^3}. \tag{8.6}$$

In (8.4), $\epsilon_m\sigma$ can be interpreted as a length scale characterizing the importance of non-continuum effects on the lubrication force between two smooth particles at close contact. Typical values of the factor ϵ_m are in the range 0.01–0.05. However, given that this term only contributes to $R_{diss}(\phi)$ through a weak logarithmic factor, its explicit

value does not play a significant role in the final results. Here, we take the typical value $\epsilon_m = 0.01$.

According to (8.1) and (8.2), the derivatives of γ and ξ with respect to n and T are given by

$$n\gamma_n = \gamma\phi\partial_\phi \ln R_{diss}(\phi), \quad \gamma_T = 0, \tag{8.7}$$

$$T\xi_T = -\tfrac{1}{2}\xi, \quad n\xi_n = \xi\phi\partial_\phi \ln S^*(\phi). \tag{8.8}$$

In particular, $n\xi_n = 0$ for a dilute suspension since $S^*(\phi) = 1$. To make a connection with the ranges of dimensionless parameters which are of practical relevance for the gas–solid flows, it is convenient to express the reduced parameters $\gamma^* \equiv (\gamma\ell)/(mv_0)$ and $\xi^* \equiv (m\xi\ell)/(Tv_0)$ in terms of the mean-flow Reynolds number Re_m and the Reynolds number associated with particle velocity fluctuations Re_T.

The expressions of γ^* and ξ^* as functions of Re_m and Re_T can easily be obtained when one takes into account (3.1), (3.2), (8.1) and (8.2). The result is

$$\gamma^* = \frac{3\pi}{\sqrt{2}\phi}\frac{\rho_g}{\rho_s}\frac{R_{diss}(\phi)}{Re_T}, \tag{8.9}$$

$$\xi^* = \frac{9}{2}\sqrt{2\pi}\left(\frac{\rho_g}{\rho_s}\right)^2 \frac{Re_m^2}{\phi\,(1-\phi)^2\,Re_T^4} S^*(\phi). \tag{8.10}$$

8.2. *Impact of gas phase on the constitutive relations*

To assess the influence of the gas phase on the constitutive relations derived in §§ 5 and 6 for the continuum equations given by (4.7)–(4.9), the zeroth- and first-order contribution to these relations ($\zeta^{(0)}$, ζ_U, η, λ, κ and μ) have been examined for spheres ($d = 3$) over a wide dimensionless parameter space: $\{\phi, \alpha, \rho_s/\rho_g, Re_m, Re_T\}$. Here, we consider a range of dimensionless parameters relevant to a CFB: $\phi = 0$–0.5, $\alpha = 0.5$–1, $\rho_s/\rho_g = 800$–2500, $Re_m = 0.1$–1 (Stokes flow), and $Re_T = 0.5$–5.

It is worthwhile to note that the results presented below are not specific to any one flow system (e.g. simple shear flow), but instead are generally applicable. In other words, all the transport coefficients are displayed as a function of the full set of dimensionless parameters, which depend on both material properties (particle mass, radius, ...) and hydrodynamic variables (granular temperature, mean relative velocity between gas and solids, ...) alike. Finally, since a primary contribution of this paper is to assess the effect of the gas phase on transport properties, the transport coefficients plotted below are non-dimensionalized with respect to their 'dry' values (those obtained when the interstitial fluid is neglected).

Recall that the gas-phase effects appear in the collisional cooling rate and transport coefficients explicitly via the appearance of γ and ξ and/or implicitly via the appearance of the kurtosis a_2, which depends on ξ via (6.25). Hence, it is worthwhile to first consider the effect of the gas phase on a_2, as is displayed in figure 5 for the representative case of $\phi = 0.1$, $Re_m = 0.5$, $Re_T = 2$, and $\rho_s/\rho_g = 1500$. It is observed that the gas phase plays a negligible role in the kurtosis a_2 since both curves (granular case and gas–solid suspension) are practically indistinguishable. Accordingly, it follows that the quantities that only have an implicit dependence on the gas phase through the appearance of a_2 also indicate a negligible role for the gas phase. These quantities include the zeroth-order collisional cooling rate $\zeta^{(0)}$ (equation (6.26)) and the bulk viscosity (equation (7.5)), which are not shown, for the sake of brevity. It is also worthwhile to note that although the first-order contribution to the collisional cooling rate ζ_U (equations (7.25)–(7.27)) and the thermal conductivity κ

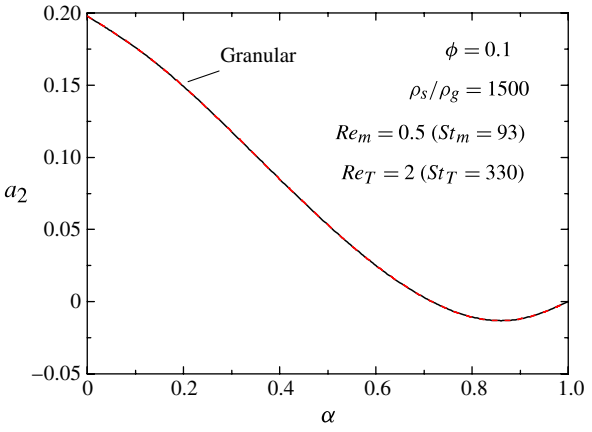

FIGURE 5. (Colour online) Fourth cumulant a_2 versus α for hard spheres with $\phi = 0.1$, $\rho_s/\rho_g = 1500$, $Re_m = 0.5$ ($St_m = 93$), and $Re_T = 2$ ($St_T = 330$). The dashed line corresponds to the results obtained in granular case (no gas phase).

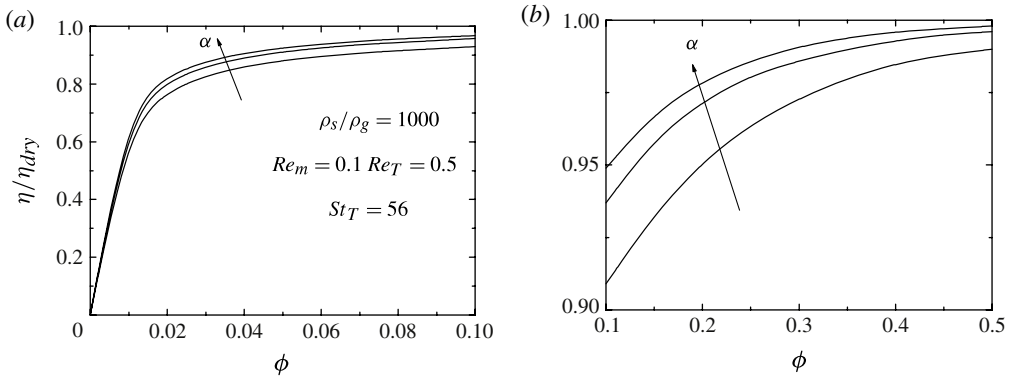

FIGURE 6. Plot of the ratio η/η_{dry} versus the volume fraction ϕ for (a) a dilute and (b) a moderately dense suspension for $\rho_s/\rho_g = 1000$, $Re_m = 0.1$, $Re_T = 0.5$ ($St_T = 56$) and three different values of the coefficient of restitution α: from bottom to top, $\alpha = 0.5, 0.7$ and 0.9.

(equations (7.14) and (7.17)) also contain an explicit dependence on γ and ξ, the gas phase shows a similarly negligible impact (<0.1 %) over the range of parameters examined. Again, for the sake of brevity these plots are not shown.

Thus, of the six constitutive quantities derived, the two for which the gas phase does exert a considerable influence are the shear viscosity η and the Dufour coefficient μ. Henceforth, the subscript *dry* refers to the value of the corresponding quantity in the absence of the gas phase (i.e. when $\beta = \gamma = \xi = 0$). The shear viscosity is displayed in figures 6 and 7. Here, the shear viscosity is shown as a function of the solid fraction ϕ for both the dilute and dense expressions (figures 6*a* and 6*b*, respectively), the density ratio ρ_s/ρ_g (figure 7*a*), the mean Reynolds number Re_m (figure 7*b*), and the Reynolds number based on particle velocity fluctuations Re_T (figure 7*c*). For each figure, only the quantity displayed along the abscissa is varied while all others are kept constant. Note also from figure 6 that the dilute- and dense-phase expressions

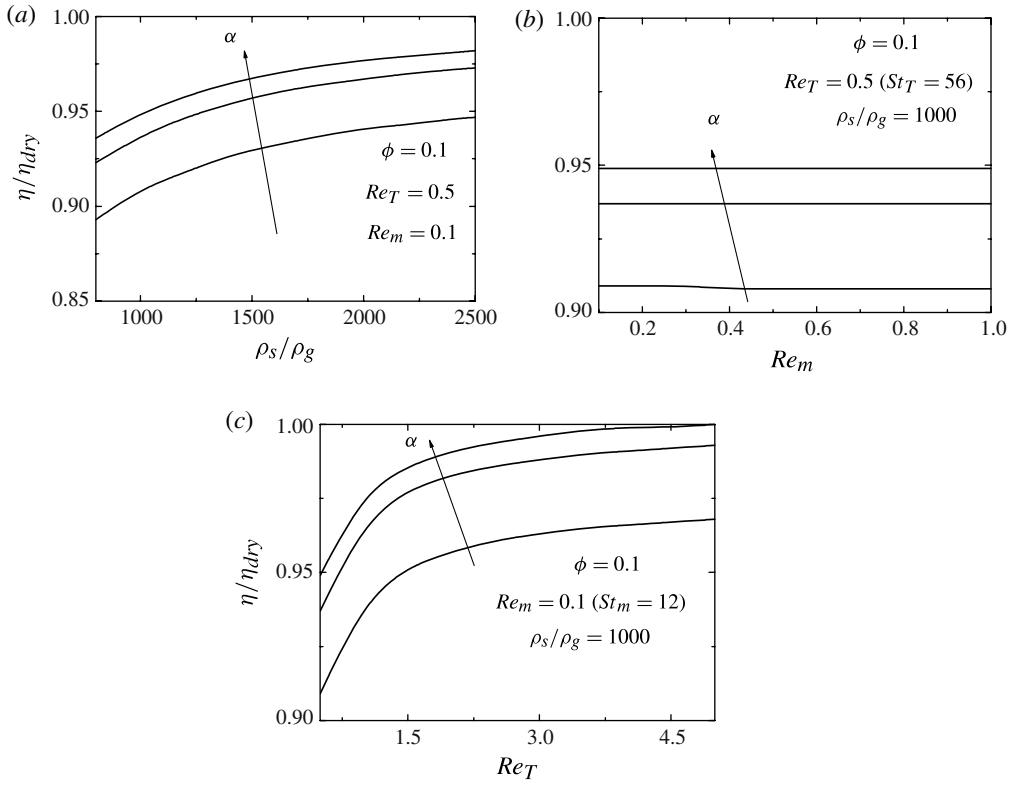

FIGURE 7. Plot of the ratio η/η_{dry} for $\phi = 0.1$ and three different values of the coefficient of restitution α: from bottom to top, $\alpha = 0.5$, 0.7 and 0.9. In (*a*) η/η_{dry} is plotted versus ρ_s/ρ_g for $Re_m = 0.1$ and $Re_T = 0.5$, in (*b*) η/η_{dry} is plotted versus Re_m for $\rho_s/\rho_g = 1000$ and $Re_T = 0.5$ ($St_T = 56$) and in (*c*) η/η_{dry} is plotted versus Re_T for $\rho_s/\rho_g = 1000$ and $Re_m = 0.1$ ($St_m = 12$).

for η/η_{dry} are roughly similar in value at the boundary of $\phi = 0.1$ used between the two sets of expressions.

Regarding the dependence of shear viscosity on concentration (figure 6*a,b*), it is observed that the dampening influence of the gas phase increases (η/η_{dry} decreases further below unity) as the system becomes more dilute (ϕ decreases), with this effect being stronger at stronger dissipation levels (lower α). The physical explanation for this behaviour is due to the increased mean free path of the particles in dilute systems, over which the gas phase serves to buffer the kinetic transport of particles. From a mathematical perspective, recall that the collisional contributions to the transport coefficients were only modified by the presence of the gas phase via the appearance of a_2, which is negligibly changed by the inclusion of a gas phase (see figure 5). On the other hand, the kinetic contribution to the shear viscosity, which dominates at more dilute conditions, has an additional dependence on the gas phase via the explicit appearance of γ and ξ (see (7.7)). It is also worthwhile to point out that the shear viscosity $\eta \to 0$ in the dilute limit, as previously reported by Tsao & Koch (1995) and Sangani *et al.* (1996). The same is not true for the granular counterpart η_{dry}, which is well known to take on a finite value in the dilute limit. Again, this behaviour can be traced to the buffering effect (viscous forces) of the interstitial gas which serves to

continually reduce the random component of particle motion in the dilute limit (the gas-phase sink of granular temperature being much larger than the gas-phase source).

Regarding the dependence of the shear viscosity on the other system parameters, figure 7(*a*) demonstrates an increased influence of the gas phase on shear viscosity as ρ_s/ρ_g decreases, which can be explained by the decreased role of particle inertia relative to gas-phase viscous forces. As displayed in figure 7(*b*), however, the shear viscosity is essentially independent of Re_m over the small range of (low) Re_m investigated here. However, as illustrated in figure 7(*c*), the gas phase displays a larger impact on the shear viscosity for lower Re_T due to the decreased role of random particle motion. At the other extreme of higher Re_T, the granular limit ($\eta/\eta_{dry} \to 1$) is approached, as expected. Finally, for all of these system parameters (figure 7*a–c*), the gas-phase effect on shear viscosity is again more pronounced for higher dissipation levels (lower α).

As discussed previously, the Reynolds numbers Re_m and Re_T can be converted to Stokes numbers St_m and St_T via (3.5) and (3.6), respectively. In figure 7, the relevant Stokes numbers both cover the range of $O(10)$–$O(100)$, though results are observed to be more sensitive to the value of St_T than St_m (i.e. figure 7*c* compared to 7*b*). In figure 7(*c*), the *x*-axis corresponds to the value of $St_T \sim 80 - 500$. At the higher St_T (higher Re_T of figure 7*c*), the shear viscosity results approach those of the dry granular limit, as expected (the fluid phase becomes negligible). However, the differences are non-negligible for St_T of $O(10)$ (lower Re_T in figure 7*c*). This observation is particularly true for more dilute systems, as illustrated in figure 6(*a*). In this figure, the Stokes number is constant at $St_T \sim 60$, yet the shear viscosity η varies greatly from its dry counterpart η_{dry}. For example, η is $\sim$40 % of η_{dry} at the volume fraction $\phi = 0.01$. Since the core of a CFB riser is often characterized by solid volume fractions of the order of a few per cent, gas-phase modifications to the shear viscosity are not negligible for practical systems, even at finite St.

Now switching to the Dufour coefficient μ, the influence of the gas phase is presented in figures 8 and 9 over similar ranges of system parameters. However, it is important to recall that $\mu = 0$ in the granular case when $\alpha = 1$. When $\alpha \neq 1$, $\mu_{dry} \neq 0$ but its magnitude is small for weak dissipation (for instance, $\mu_{dry} \simeq 0.207$ for $\alpha = 0.9$ and $\phi = 0.2$). In stark contrast to the shear viscosity (figures 6 and 7), the gas phase serves to increase the Dufour coefficient relative to its dry counterpart (i.e. $\mu/\mu_{dry} > 1$), and these effects are more noticeable at lower dissipation levels (higher α). Nonetheless, similar to the shear viscosity, the influence of the gas phase is greater at more dilute conditions since the kinetic contributions dominate over their collisional counterparts (figure 8*a,b*). Also similar is the increased role of the gas phase for lower density ratios due to the decreased role of particle inertia (figure 9*a*). Finally, the impact of Re_T and Re_m on the Dufour coefficient is analogous to that of the shear viscosity, where the influence of the gas phase is relatively independent of Re_m (see figure 9*b*) over the range of low Re_m considered, but does depend on Re_T (see figure 9*c*).

The behaviour of the Dufour coefficient in the elastic limit ($\alpha = 1$) is further explored in figure 10. Recall that for the dry granular case (no gas phase) $\mu = 0$ at $\alpha = 1$, so the discovery of a non-zero value for the gas–solid suspension may appear surprising. However, the appearance of a non-zero Dufour coefficient is also observed in granular mixtures (i.e. more than one solid species) at the elastic limit (see e.g. Garzó, Dufty & Hrenya 2007*a*; Garzó, Hrenya & Dufty 2007*b*), so the gas phase plays an analogous role to an additional solid species in this regard. As illustrated in figure 10, μ increases with solid fraction but decreases with Re_T; note

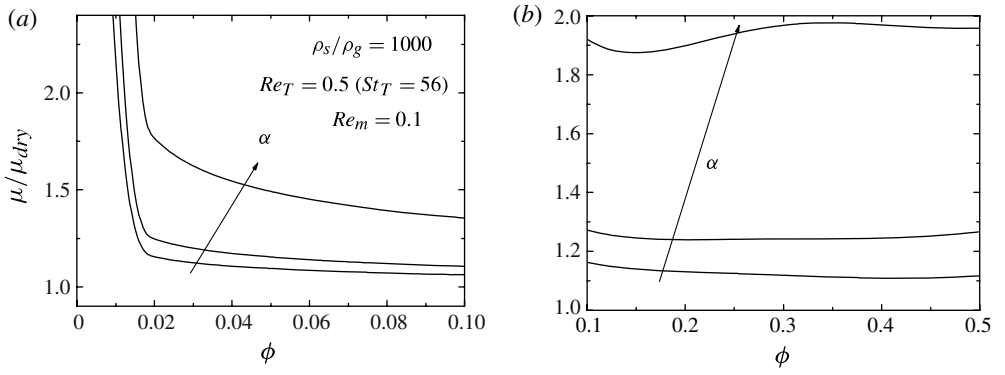

FIGURE 8. Plot of the ratio μ/μ_{dry} versus the volume fraction ϕ for (*a*) a dilute and (*b*) a moderately dense suspension for $\rho_s/\rho_g = 1000$, $Re_m = 0.1$, $Re_T = 0.5$ ($St_T = 56$) and three different values of the coefficient of restitution α: from bottom to top, $\alpha = 0.5$, 0.7 and 0.9.

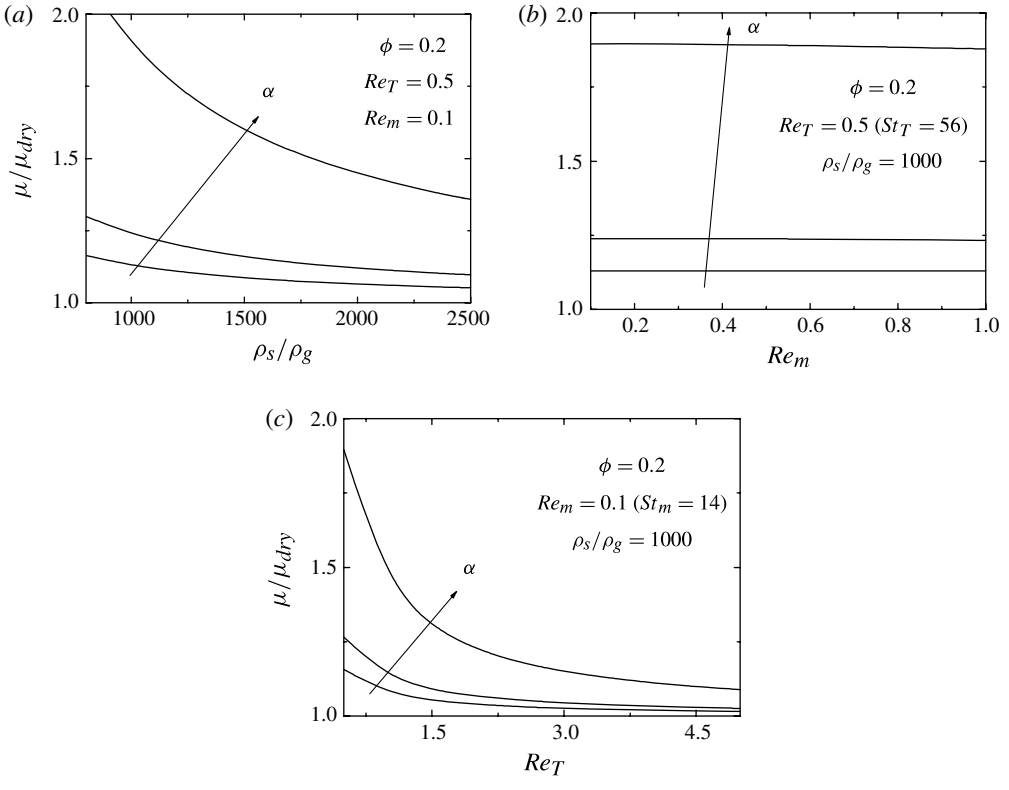

FIGURE 9. Plot of the ratio μ/μ_{dry} for $\phi = 0.2$ and three different values of the coefficient of restitution α: from bottom to top, α=0.5, 0.7 and 0.9. In (*a*) μ/μ_{dry} is plotted versus ρ_s/ρ_g for $Re_m = 0.1$ and $Re_T = 0.5$, in (*b*) η/η_{dry} is plotted versus Re_m for $\rho_s/\rho_g = 1000$ and $Re_T = 0.5$ ($St_T = 56$) and in (*c*) μ/μ_{dry} is plotted versus Re_T for $\rho_s/\rho_g = 1000$ and $Re_m = 0.1$ ($St_m = 14$).

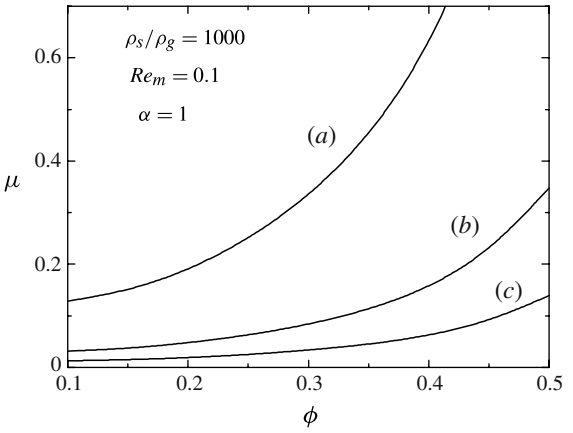

FIGURE 10. Plot of the Dufour coefficient μ versus ϕ for hard spheres with $\alpha = 1$ (elastic collisions), $Re_m = 0.5$, $\rho_s/\rho_g = 1000$, and three different values of the Reynolds number Re_T: (*a*) $Re_T = 0.5$ ($St_T = 56$), (*b*) $Re_T = 2$ ($St_T = 222$), and (*c*) $Re_T = 5$ ($St_T = 556$).

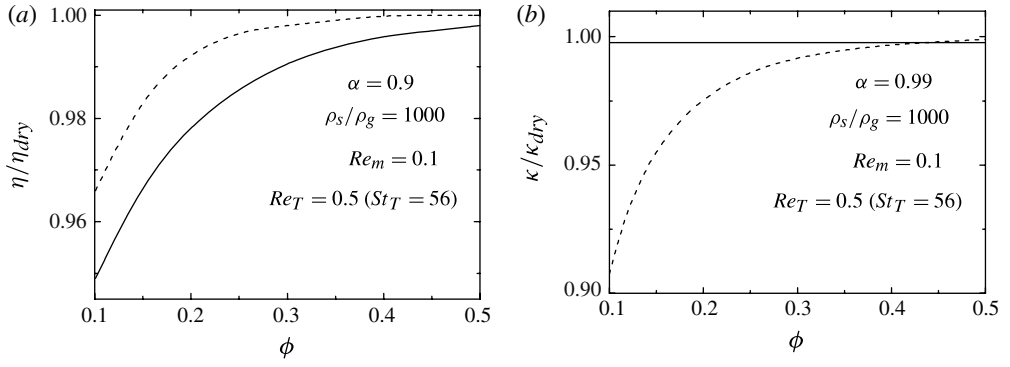

FIGURE 11. Plot of the ratios (*a*) η/η_{dry} and (*b*) κ/κ_{dry} as a function of the solid fraction ϕ for $Re_m = 0.1$, $Re_T = 0.5$ ($St_T = 56$) and different values of the coefficient of restitution α. The solid lines are the results derived here while the dashed lines are based on the model used by Agrawal *et al.* (2001).

that this trend cannot be compared with that of figure 8 directly since the latter is non-dimensionalized with the dry case and figure 10 is not to avoid division by zero.

Although the previous analytical works of Koch and co-workers in the Stokes flow limit (Koch 1990; Sangani *et al.* 1996; Koch & Sangani 1999) ignore the impact of the gas phase on the solid-phase constitutive relations, other groups have included such effects (Ma & Ahmadi 1988; Balzer *et al.* 1995; Lun & Savage 2003). Expressions including such effects for shear viscosity and thermal conductivity are given by Agrawal *et al.* (2001), and are compared with those derived here in figures 11(*a*) and 11(*b*), respectively. For the shear viscosity (figure 11*a*), the qualitative nature of the gas-phase influence is similar in that it is more apparent at dilute conditions, though the expression derived here shows a stronger gas-phase influence. On the other hand, for the case of the thermal conductivity (figure 11*b*), the expression derived here displays essentially no impact from the gas phase, whereas previous expressions

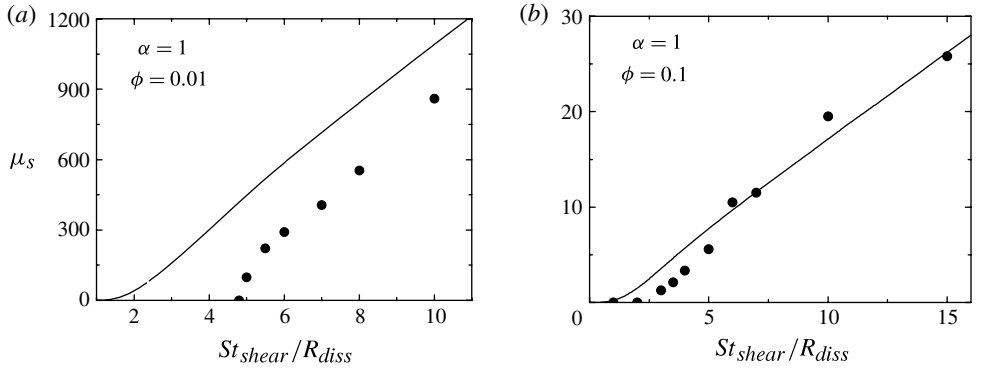

FIGURE 12. Plot of reduced shear viscosity $\mu_s = 4\eta/(\rho_s\phi\dot{\gamma}\sigma^2)$ as a function of St_{shear}/R_{diss} in the case of hard spheres with $\alpha = 1$ for two different values of the solid volume fraction: (*a*) $\phi = 0.01$ and (*b*) $\phi = 0.1$. The solid lines are the theoretical results and the circles are the simulation results obtained by Sangani *et al.* (1996).

show a dampening of the thermal conductivity relative to the (dry) granular case. It is worth noting, however, that this comparison is not apples-to-apples due to two key differences between the previous treatments and the current one. Namely, as described in § 1, the previous treatments have incorporated the effects of gas-phase turbulence and have used a form of the instantaneous drag force that mimics the form of the mean force, neither of which is implemented in our expressions.

Finally, our predictions for the shear viscosity and the steady granular temperature are compared in figures 12 and 13, respectively, with the numerical simulations performed by Sangani *et al.* (1996). The shear viscosity and the (steady) granular temperature were obtained from simulations in the simple shear flow state, and thus $Re_m = 0$. Consistent with this work (Sangani *et al.* 1996), the results here are plotted against a Stokes number St_{shear} based on the shear rate $\dot{\gamma} \equiv \partial U_x/\partial y$. This Stokes number is defined by (Sangani *et al.* 1996)

$$St_{shear} = \frac{m\dot{\gamma}}{3\pi\sigma\mu_g}. \tag{8.11}$$

The reduced shear viscosity μ_s is defined by

$$\mu_s = \frac{4\eta}{\rho_s\phi\dot{\gamma}\sigma^2}, \tag{8.12}$$

while the (steady) granular temperature θ is

$$\theta = \frac{4T}{m\sigma^2\dot{\gamma}^2}. \tag{8.13}$$

In the simple shear flow state, the granular temperature T is determined by applying the steady-state condition to the balance equation of the temperature. The shear viscosity μ_s and the square root of temperature $\sqrt{\theta}$ are plotted in figures 12 and 13, respectively, as functions of St_{shear}/R_{diss} for hard spheres with $\alpha = 1$. (Note that the reduced shear viscosity μ_s is also defined differently than shown in Sangani *et al.* (1996). The results presented here correct the error contained in the original publication; D. L. Koch, personal communication.) It is apparent that our theoretical

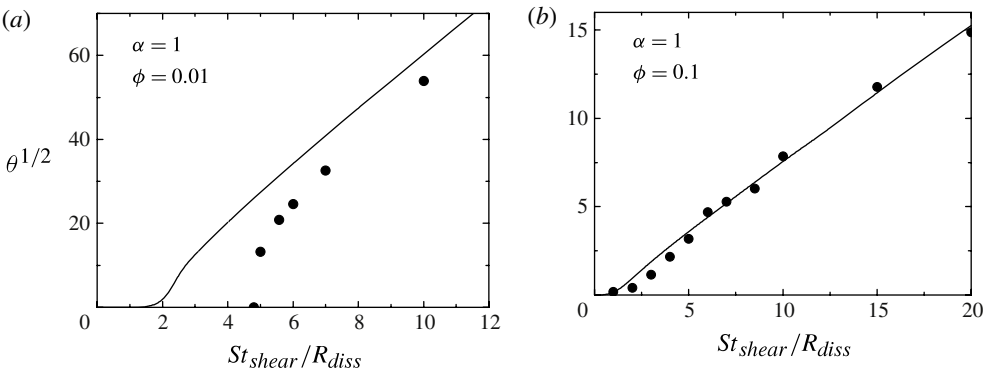

FIGURE 13. Plot of the square root of granular temperature $\sqrt{\theta} = \sqrt{4T/m}\,(\dot{\gamma}\sigma)^{-1}$ as a function of St_{shear}/R_{diss} in the case of hard spheres with $\alpha = 1$ for two different values of the solid volume fraction: (*a*) $\phi = 0.01$ and (*b*) $\phi = 0.1$. The solid lines are the theoretical results and the circles are the simulation results obtained by Sangani *et al.* (1996).

predictions slightly overestimate the shear viscosity and granular temperature for dilute conditions ($\phi = 0.01$ in figures 12*a* and 13*a*) while exhibiting close agreement at more moderate volume fractions ($\phi = 0.1$ in figures 12*b* and 13*b*). This observation can be explained via the assumption of low Knudsen number Kn used in our derivation. In particular, previous work in granular systems (no fluid phase) has shown that the simple shear flow state contains higher-order effects (beyond Navier–Stokes order: see Santos *et al.* 2004) and that such effects become more important in dilute flows (Hrenya *et al.* 2008). Nonetheless, the agreement here is encouraging and bodes well for the extension of the PR–DNS-based acceleration model used here to higher Re_m, and its subsequent incorporation into Navier–Stokes-order hydrodynamics, especially considering the complexities associated with deriving higher-order hydrodynamics and associated boundary conditions.

9. Summary

In this work, a rigorous incorporation of the gas phase into the starting kinetic (Enskog) equation has been demonstrated via an instantaneous model for the drag force. A unique aspect of this work is the use of a Langevin model for the instantaneous gas-phase force on a particle. Here we have focused on a parameter space consistent with the conditions of a CFB (i.e. $\phi = 0$–$0.5, \alpha = 0.5$–1, $\rho_s/\rho_g =$ 800–2500, $Re_m = 0.1$–1 and $Re_T = 0.5$–5). The coefficients of the Langevin model are related to the dissipation and source of granular energy and can be obtained from analytical expressions (for Stokes flow and $\phi < 0.1$: Koch 1990) or from simulations (multipole expansions for Stokes flow and $\phi > 0.1$: Koch & Sangani 1999) or from PR–DNS (for higher Reynolds numbers). For proof-of-concept purposes, attention here is limited to low Reynolds numbers in order to allow for direct comparisons with previous analytical treatments. It is found that the additional terms appearing in the balance equations due to the presence of the gas phase are the same regardless of treatment. Furthermore, the Chapman–Enskog method is used to derive Navier–Stokes-order constitutive relations for balance equations. The results indicate a non-negligible influence of the gas phase on the shear viscosity and the Dufour coefficient, whereas such effects had been ignored in previous analytical treatments for Stokes flow.

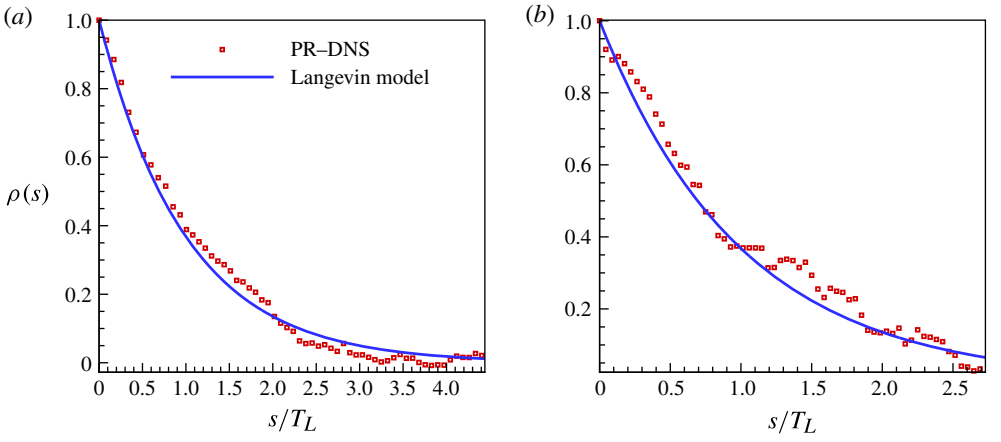

FIGURE 14. (Colour online) Plots showing the verification of the Langevin model. (*a*) The particle velocity autocorrelation function extracted from PR–DNS of freely evolving suspension (volume fraction of 0.2, mean-flow Reynolds number 20 and solid-to-fluid density ratio of 100) compared with the exponential decay predicted by the Langevin model. (*b*) The same as (*a*) for a suspension with solid-to-fluid density of 100.

Specifically, the presence of the gas phase lowers the shear viscosity and increases the Dufour coefficient relative to the granular (no gas phase) case, with the degree of influence larger in more dilute systems. This non-negligible influence persists even for finite Stokes number of $O(10)$. Moreover, the shear viscosity in gas–solid suspensions is found to approach to zero in the dilute limit (consistent with previous findings of Tsao & Koch 1995 and Sangani *et al.* 1996 for simple shear flow), unlike its granular counterpart which takes on a finite value in the same limit. Also, the Dufour coefficient in gas–solid systems is found to be non-zero in the elastic limit, which is not the case for (dry) granular systems but is the case for granular mixtures (i.e. more than one solid species).

The Langevin model for the instantaneous gas–solid force is applicable to a much wider parameter space than that explored here, including higher Reynolds numbers and polydisperse systems. For instance, figure 14 shows that the decay of the particle velocity autocorrelation function $\rho(s)$ (see equation (3.7)) computed by PR–DNS of freely evolving gas–solid suspension at a mean-flow Reynolds number of 20 matches the exponential decay predicted by the Langevin equation. Therefore, fluid–solid force models of the form given by (2.1) can be extended seamlessly to gas–solid systems at higher Reynolds numbers. The model coefficients for such systems are attainable via PR–DNS, which are not limited to a narrow parameter space as is their analytical counterpart. Such work is expected to be important for a wide range of practical applications and physical phenomena, such as systems in which the interstitial gas has been shown to have an impact on the stability of the homogeneous state (Koch 1990; Garzó 2005) or on species segregation (Möbius *et al.* 2001; Naylor, Swift & King 2003; Yan *et al.* 2003; Sánchez, Swift & King 2004; Möbius *et al.* 2005; Wylie *et al.* 2008; Zeilstra, van der Hoef & Kuipers 2008; Idler *et al.* 2009; Clement *et al.* 2010). Finally, this work serves as a proof-of-concept for the use of PR–DNS-based models for instantaneous particle acceleration in the starting kinetic equation; this approach can in principle be extended to more complex flows such as those requiring an anisotropic Langevin model.

Acknowledgements

The work of V.G. has been supported by the Ministerio de Educacion y Ciencia (Spain) through Grant FIS2010-16587, partially financed by FEDER funds and by the Junta de Extremadura (Spain) through Grant GR10158. C.M.H. and S.S. are grateful for the funding support provided by the US Department of Energy (DE-FC26-07NT43098). C.M.H. would also like to acknowledge funding from the National Science Foundation (CBET-0318999). S.S. would like to acknowledge funding from the National Science Foundation (CBET-1134500).

Appendix A. Chapman–Enskog method

The velocity distribution function $f^{(1)}$ obeys the kinetic equation

$$\left(\partial_t^{(0)}+\mathscr{L}\right)f^{(1)}-\left(\frac{\beta}{m}\Delta\boldsymbol{U}-\boldsymbol{g}\right)\cdot\frac{\partial f^{(1)}}{\partial\boldsymbol{V}}-\frac{\gamma}{m}\frac{\partial}{\partial\boldsymbol{V}}\cdot\boldsymbol{V}f^{(1)}-\frac{1}{2}\xi\frac{\partial^2}{\partial V^2}f^{(1)}$$
$$=-\left(\partial_t^{(1)}+\boldsymbol{v}\cdot\boldsymbol{\nabla}\right)f^{(0)}-J_E^{(1)}[f]. \tag{A 1}$$

Here, $J_E^{(1)}[f]$ means the first-order contribution to the expansion of the Enskog collision operator and $\mathscr{L}$ is the linear operator

$$\mathscr{L}f^{(1)}=-\left(J_E^{(0)}[f^{(0)},f^{(1)}]+J_E^{(0)}[f^{(1)},f^{(0)}]\right). \tag{A 2}$$

The macroscopic balance equations to first order in the gradients are

$$D_t^{(1)}n=-n\boldsymbol{\nabla}\cdot\boldsymbol{U},\quad D_t^{(1)}U_i=-(mn)^{-1}\boldsymbol{\nabla}_i p,\quad D_t^{(1)}T=-\frac{2p}{\mathrm{d}n}\boldsymbol{\nabla}\cdot\boldsymbol{U}-\zeta^{(1)}T, \tag{A 3}$$

where $D_t^{(1)}\equiv\partial_t^{(1)}+\boldsymbol{U}\cdot\boldsymbol{\nabla}$. Use of (A 3) in (A 1) and taking into account the form of $J_E^{(1)}[f]$ obtained by Garzó & Dufty (1999) for a dry granular gas, one gets

$$\left(\partial_t^{(0)}+\mathscr{L}\right)f^{(1)}-\left(\frac{\beta}{m}\Delta\boldsymbol{U}-\boldsymbol{g}\right)\cdot\frac{\partial f^{(1)}}{\partial\boldsymbol{V}}-\frac{\gamma}{m}\frac{\partial}{\partial\boldsymbol{V}}\cdot\boldsymbol{V}f^{(1)}-\frac{1}{2}\xi\frac{\partial^2}{\partial V^2}f^{(1)}$$
$$=\boldsymbol{A}\cdot\boldsymbol{\nabla}\ln T+\boldsymbol{B}\cdot\boldsymbol{\nabla}\ln n+C_{ij}\frac{1}{2}\left(\partial_i U_j+\partial_j U_i-\frac{2}{d}\delta_{ij}\boldsymbol{\nabla}\cdot\boldsymbol{U}\right)+D\boldsymbol{\nabla}\cdot\boldsymbol{U}, \tag{A 4}$$

where the expressions of $\boldsymbol{A}$, $\boldsymbol{B}$, C_{ij} and D are the same as those obtained by Garzó & Dufty (1999). They are given by

$$A_i(\boldsymbol{V})=\frac{1}{2}V_i\boldsymbol{\nabla}_V\cdot\boldsymbol{V}f^{(0)}-\frac{p}{\rho}\frac{\partial}{\partial V_i}f^{(0)}+\frac{1}{2}\mathscr{K}_i\left[\boldsymbol{\nabla}_V\cdot\left(\boldsymbol{V}f^{(0)}\right)\right], \tag{A 5}$$

$$B_i(\boldsymbol{V})=-V_i f^{(0)}-\frac{p}{\rho}\left(1+\phi\frac{\partial}{\partial\phi}\ln p^*\right)\frac{\partial}{\partial V_i}f^{(0)})-\left(1+\frac{1}{2}\phi\frac{\partial}{\partial\phi}\ln\chi\right)\mathscr{K}_i\left[f^{(0)}\right], \tag{A 6}$$

$$C_{ij}(\boldsymbol{V})=V_i\frac{\partial}{\partial V_j}f^{(0)}+\mathscr{K}_i\left[\frac{\partial}{\partial V_j}f^{(0)}\right], \tag{A 7}$$

$$D=\frac{1}{d}\boldsymbol{\nabla}_V\cdot\left(\boldsymbol{V}f^{(0)}\right)-\frac{1}{2}\left(\zeta_U+\frac{2}{d}p^*\right)\boldsymbol{\nabla}_V\cdot\left(\boldsymbol{V}f^{(0)}\right)+\frac{1}{d}\mathscr{K}_i\left[\partial_{V_i}f^{(0)}\right]. \tag{A 8}$$

Here, $\boldsymbol{\nabla}_V\equiv\partial/\partial\boldsymbol{V}$,

$$p^*\equiv\frac{p}{n\boldsymbol{T}}=1+2^{d-2}(1+\alpha)\chi\phi, \tag{A 9}$$

ϕ is defined by (6.15), ζ_U is defined by (7.24) and (7.25) and $\mathscr{K}_i$ is the operator

$$\mathscr{K}_i[X] = \sigma^d \chi \int \mathrm{d}\boldsymbol{v}_2 \int \mathrm{d}\,\widehat{\boldsymbol{\sigma}}\,\Theta(\widehat{\boldsymbol{\sigma}}\cdot\boldsymbol{g}_{12})(\widehat{\boldsymbol{\sigma}}\cdot\boldsymbol{g}_{12})\widehat{\sigma}_i \times \left[\alpha^{-2} f^{(0)}(\boldsymbol{v}_1'')X(\boldsymbol{v}_2'') + f^{(0)}(\boldsymbol{v}_1)X(\boldsymbol{v}_2)\right], \tag{A 10}$$

where $\boldsymbol{v}_1'' = \boldsymbol{v}_1 - ((1+\alpha^{-1})(\widehat{\boldsymbol{\sigma}}\cdot\boldsymbol{g}_{12})\widehat{\boldsymbol{\sigma}}/2)$ and $\boldsymbol{v}_2'' = \boldsymbol{v}_2 + ((1+\alpha^{-1})(\widehat{\boldsymbol{\sigma}}\cdot\boldsymbol{g}_{12})\widehat{\boldsymbol{\sigma}}/2)$.

The solution to (A 4) can be written in the form (7.1). The unknown functions of the peculiar velocity, $\boldsymbol{\mathcal{A}}$, $\boldsymbol{\mathcal{B}}$, $\mathscr{C}_{ij}$ and $\mathscr{D}$ appearing in $f^{(1)}$ are determined by solving (A 4). By dimensional analysis, $\boldsymbol{\mathcal{A}}(\boldsymbol{V}) = v_0^{-d}\ell^{1-d}\boldsymbol{\mathcal{A}}^*(\boldsymbol{V}^*)$, $\boldsymbol{\mathcal{B}}(\boldsymbol{V}) = v_0^{-d}\ell^{1-d}\boldsymbol{\mathcal{B}}^*(\boldsymbol{V}^*)$, $\mathscr{C}_{ij}(\boldsymbol{V}) = v_0^{-(d+1)}\ell^{1-d}\mathscr{C}_{ij}^*(\boldsymbol{V}^*)$ and $\mathscr{D}(\boldsymbol{V}) = v_0^{-(d+1)}\ell^{1-d}\mathscr{D}^*(\boldsymbol{V}^*)$, where $\ell = 1/n\sigma^{d-1}$ is the mean free path for hard spheres and $\boldsymbol{\mathcal{A}}^*(\boldsymbol{V}^*)$, $\boldsymbol{\mathcal{B}}^*(\boldsymbol{V}^*)$, $\mathscr{C}_{ij}^*(\boldsymbol{V}^*)$, and $\mathscr{D}_i^*(\boldsymbol{V}^*)$ are dimensionless functions of the reduced velocity $\boldsymbol{V}^* = \boldsymbol{V}/v_0$, $v_0 = \sqrt{2T/m}$ being the thermal speed. Consequently,

$$\partial_t^{(0)}\boldsymbol{\mathcal{A}}(\boldsymbol{V}) = (\partial_t^{(0)}T)\partial_T\boldsymbol{\mathcal{A}}(\boldsymbol{V}) = -\frac{1}{2T}\nabla_{\boldsymbol{V}}\cdot(\boldsymbol{V}\boldsymbol{\mathcal{A}}(\boldsymbol{V}))(\partial_t^{(0)}T) = -\frac{1}{2T}\nabla_{\boldsymbol{V}}\cdot(\boldsymbol{V}\boldsymbol{\mathcal{A}}(\boldsymbol{V}))\left(m\xi - \frac{2T}{m}\gamma - \zeta^{(0)}T\right), \tag{A 11}$$

$$\partial_t^{(0)}\boldsymbol{\mathcal{B}}(\boldsymbol{V}) = (\partial_t^{(0)}T)\partial_T\boldsymbol{\mathcal{B}}(\boldsymbol{V}) = -\frac{1}{2T}\nabla_{\boldsymbol{V}}\cdot(\boldsymbol{V}\boldsymbol{\mathcal{B}}(\boldsymbol{V}))(\partial_t^{(0)}T) = -\frac{1}{2T}\nabla_{\boldsymbol{V}}\cdot(\boldsymbol{V}\boldsymbol{\mathcal{B}}(\boldsymbol{V}))\left(m\xi - \frac{2T}{m}\gamma - \zeta^{(0)}T\right), \tag{A 12}$$

$$\partial_t^{(0)}\mathscr{C}_{ij}(\boldsymbol{V}) = (\partial_t^{(0)}T)\partial_T\mathscr{C}_{ij}(\boldsymbol{V}) = -\frac{1}{2T}\left[\nabla_{\boldsymbol{V}}\cdot\left(\boldsymbol{V}\mathscr{C}_{ij}(\boldsymbol{V})\right) + \mathscr{C}_{ij}\right](\partial_t^{(0)}T) = -\frac{1}{2T}\left[\nabla_{\boldsymbol{V}}\cdot\left(\boldsymbol{V}\mathscr{C}_{ij}(\boldsymbol{V})\right) + \mathscr{C}_{ij}\right]\left(m\xi - \frac{2T}{m}\gamma - \zeta^{(0)}T\right), \tag{A 13}$$

$$\partial_t^{(0)}\mathscr{D}(\boldsymbol{V}) = (\partial_t^{(0)}T)\partial_T\mathscr{D}(\boldsymbol{V}) = -\frac{1}{2T}\left[\nabla_{\boldsymbol{V}}\cdot(\boldsymbol{V}\mathscr{D}(\boldsymbol{V})) + \mathscr{D}\right](\partial_t^{(0)}T) = -\frac{1}{2T}\left[\nabla_{\boldsymbol{V}}\cdot(\boldsymbol{V}\mathscr{D}(\boldsymbol{V})) + \mathscr{D}\right]\left(m\xi - \frac{2T}{m}\gamma - \zeta^{(0)}T\right). \tag{A 14}$$

In addition,

$$\partial_t^{(0)}\nabla\ln T = \nabla\partial_t^{(0)}\ln T = \nabla\left(\frac{m\xi}{T} - \frac{2}{m}\gamma - \zeta^{(0)}\right) = -\left[\frac{2n}{m}\gamma_n - \frac{\rho}{T}\xi_n + \zeta^{(0)}\left(1 + \phi\partial_\phi\ln\chi\right)\right]\nabla\ln n - \left(\frac{2T}{m}\gamma_T + \frac{m}{T}\xi - m\xi_T + \frac{1}{2}\zeta^{(0)}\right)\nabla\ln T, \tag{A 15}$$

where

$$\gamma_n \equiv \frac{\partial\gamma}{\partial n}, \quad \gamma_T \equiv \frac{\partial\gamma}{\partial T}, \tag{A 16}$$

$$\xi_n \equiv \frac{\partial\xi}{\partial n}, \quad \xi_T \equiv \frac{\partial\xi}{\partial T}. \tag{A 17}$$

Upon deriving (A 14), use has been made of the explicit form of $\zeta^{(0)}$. Since the gradients of the fields are all independent, (A 4) can be separated into independent equations for each coefficient. This leads to the following set of linear, inhomogeneous integral equations:

$$\frac{1}{2}\left(\frac{2\gamma}{m}-\frac{m\xi}{T}+\zeta^{(0)}\right)\frac{\partial}{\partial \boldsymbol{V}}\cdot(\boldsymbol{V}\mathcal{A})-\left(\frac{2T}{m}\gamma_T+\frac{m}{T}\xi-m\xi_T+\frac{1}{2}\zeta^{(0)}\right)\mathcal{A}$$
$$-\left(\frac{\beta}{m}\Delta\boldsymbol{U}-\boldsymbol{g}\right)\cdot\frac{\partial}{\partial \boldsymbol{V}}\mathcal{A}-\frac{\gamma}{m}\frac{\partial}{\partial \boldsymbol{V}}\cdot\boldsymbol{V}\mathcal{A}-\frac{1}{2}\xi\frac{\partial^2}{\partial V^2}\mathcal{A}+\mathscr{L}\mathcal{A}=\boldsymbol{A}, \tag{A 18}$$

$$\frac{1}{2}\left(\frac{2\gamma}{m}-\frac{m\xi}{T}+\zeta^{(0)}\right)\frac{\partial}{\partial \boldsymbol{V}}\cdot(\boldsymbol{V}\mathcal{B})-\left(\frac{\beta}{m}\Delta\boldsymbol{U}-\boldsymbol{g}\right)\cdot\frac{\partial}{\partial \boldsymbol{V}}\mathcal{B}$$
$$-\frac{\gamma}{m}\frac{\partial}{\partial \boldsymbol{V}}\cdot\boldsymbol{V}\mathcal{B}-\frac{1}{2}\xi\frac{\partial^2}{\partial V^2}\mathcal{B}+\mathscr{L}\mathcal{B}=\boldsymbol{B}$$
$$+\left[\frac{2n}{m}\gamma_n-\frac{\rho}{T}\xi_n+\zeta^{(0)}\left(1+\phi\partial_\phi\ln\chi\right)\right]\mathcal{A}, \tag{A 19}$$

$$\frac{1}{2}\left(\frac{2\gamma}{m}-\frac{m\xi}{T}+\zeta^{(0)}\right)\left[\mathscr{C}_{ij}+\frac{\partial}{\partial \boldsymbol{V}}\cdot\left(\boldsymbol{V}\mathscr{C}_{ij}\right)\right]-\left(\frac{\beta}{m}\Delta\boldsymbol{U}-\boldsymbol{g}\right)\cdot\frac{\partial}{\partial \boldsymbol{V}}\mathscr{C}_{ij}$$
$$-\frac{\gamma}{m}\frac{\partial}{\partial \boldsymbol{V}}\cdot\boldsymbol{V}\mathscr{C}_{ij}-\frac{1}{2}\xi\frac{\partial^2}{\partial V^2}\mathscr{C}_{ij}+\mathscr{L}\mathscr{C}_{ij}=C_{ij}, \tag{A 20}$$

$$\frac{1}{2}\left(\frac{2\gamma}{m}-\frac{m\xi}{T}+\zeta^{(0)}\right)\left[\mathscr{D}+\frac{\partial}{\partial \boldsymbol{V}}\cdot(\boldsymbol{V}\mathscr{D})\right]-\left(\frac{\beta}{m}\Delta\boldsymbol{U}-\boldsymbol{g}\right)\cdot\frac{\partial}{\partial \boldsymbol{V}}\mathscr{D}$$
$$-\frac{\gamma}{m}\frac{\partial}{\partial \boldsymbol{V}}\cdot\boldsymbol{V}\mathscr{D}-\frac{1}{2}\xi\frac{\partial^2}{\partial V^2}\mathscr{D}+\mathscr{L}\mathscr{D}=D. \tag{A 21}$$

Equations (A 18)–(A 21) reduce to those previously obtained for dry granular fluids (no gas phase) (Garzó & Dufty 1999; Lutsko 2005) when $\beta=\gamma=\xi=0$.

Appendix B. Kinetic contributions and collisional cooling rate

In this appendix we give some details of the evaluation of the kinetic contributions to the transport coefficients η, κ and μ and the first-order contribution ζ_U to the collisional cooling rate.

Let us start with the shear viscosity η. Its kinetic part η_k is given by

$$\eta_k=-\frac{1}{(d-1)(d+2)}\int \mathrm{d}\boldsymbol{v}\, D_{ij}\mathscr{C}_{ij}(\boldsymbol{V}), \tag{B 1}$$

where $D_{ij}=m(V_iV_j-(1/d)V^2\delta_{ij})$. To obtain it, we multiply (A 19) by D_{ij} and integrate over velocity to get

$$-\frac{1}{2}\left(\frac{2\gamma}{m}-\frac{m\xi}{T}+\zeta^{(0)}\right)\eta_k+\frac{2\gamma}{m}\eta_k+\nu_\eta\eta_k=nT$$
$$-\frac{1}{(d-1)(d+2)}\int \mathrm{d}\boldsymbol{V}D_{ij}(\boldsymbol{V})\mathscr{K}_i\left[\frac{\partial}{\partial V_j}f^{(0)}\right], \tag{B 2}$$

where

$$\nu_\eta = \frac{\int \mathrm{d}\boldsymbol{v}\, D_{ij}(\boldsymbol{V})\mathscr{L}\mathscr{C}_{ij}(\boldsymbol{V})}{\int \mathrm{d}\boldsymbol{v}\, D_{ij}(\boldsymbol{V})\mathscr{C}_{ij}(\boldsymbol{V})}, \tag{B 3}$$

and use has been made of the results

$$\int \mathrm{d}\boldsymbol{V} D_{ij}\frac{\partial}{\partial V_\ell}\mathscr{C}_{ij} = 0, \quad \int \mathrm{d}\boldsymbol{V} D_{ij}\frac{\partial}{\partial V_\ell}V_\ell\mathscr{C}_{ij} = 2(d-1)(d+2)\eta_k, \tag{B 4}$$

$$\int \mathrm{d}\boldsymbol{V} D_{ij}\frac{\partial^2}{\partial V^2}\mathscr{C}_{ij} = 0. \tag{B 5}$$

The first identity in (B 4) and (B 5) follow from the solubility conditions of the Chapman–Enskog method:

$$\int \mathrm{d}\boldsymbol{v}\{1, \boldsymbol{v}, v^2\}f^{(1)}(\boldsymbol{V}) = \{0, \boldsymbol{0}, 0\}. \tag{B 6}$$

The collision integral of the right-hand side of (B 2) has been evaluated in previous works (Garzó & Dufty 1999; Lutsko 2005). Thus, the kinetic part η_k is given by

$$\eta_k = \frac{nT}{\nu_\eta - \frac{1}{2}\left(\zeta^{(0)} - \frac{m}{T}\xi - \frac{2}{m}\gamma\right)}\left[1 - \frac{2^{d-2}}{d+2}(1+\alpha)(1-3\alpha)\phi\chi\right]. \tag{B 7}$$

In order to get an explicit expression for η_k, one has to consider the leading terms in a Sonine polynomial expansion of the distribution function. Here, we have considered a recent modified version of the standard method (Garzó *et al.* 2007*c*; Garzó, Vega Reyes & Montanero 2009) that yields good agreement with computer simulations even for quite strong values of dissipation (Montanero, Santos & Garzó 2007). The final form of η_k is given by (7.7).

The kinetic parts κ_k and μ_k of the transport coefficients characterizing the heat flux are defined, respectively, as

$$\kappa_k = -\frac{1}{\mathrm{d}T}\int \mathrm{d}\boldsymbol{v}\boldsymbol{S}(\boldsymbol{V})\cdot\boldsymbol{\mathcal{A}}(\boldsymbol{V}), \tag{B 8}$$

$$\mu_k = -\frac{1}{\mathrm{d}n}\int \mathrm{d}\boldsymbol{v}\,\boldsymbol{S}(\boldsymbol{V})\cdot\boldsymbol{\mathcal{B}}(\boldsymbol{V}), \tag{B 9}$$

where

$$\boldsymbol{S}(\boldsymbol{V}) = \left(\frac{m}{2}V^2 - \frac{d+2}{2}T\right)\boldsymbol{V}. \tag{B 10}$$

We obtain first the kinetic part κ_k. It is obtained by multiplying (A 18) by $\boldsymbol{S}(\boldsymbol{V})$ and integrating over $\boldsymbol{V}$. The result is

$$-\frac{3}{2}\left(\frac{2\gamma}{m} - \frac{m\xi}{T} + \zeta^{(0)}\right)\kappa_k - \left(\frac{2T}{m}\gamma_T + \frac{m}{T}\xi - m\xi_T + \frac{1}{2}\zeta^{(0)}\right)\kappa_k$$
$$+\left(\frac{3\gamma}{m} + \nu_\kappa\right)\kappa_k = -\frac{1}{\mathrm{d}T}\int \mathrm{d}\boldsymbol{V}\,\boldsymbol{S}(\boldsymbol{V})\cdot\boldsymbol{A}, \tag{B 11}$$

where

$$\nu_\kappa = \frac{\int d\boldsymbol{v}\, \boldsymbol{S}(\boldsymbol{V})\cdot \mathscr{L}\boldsymbol{\mathcal{A}}(\boldsymbol{V})}{\int d\boldsymbol{v}\, \boldsymbol{S}(\boldsymbol{V})\boldsymbol{\mathcal{A}}(\boldsymbol{V})}, \tag{B 12}$$

and use has been made of the results

$$\int d\boldsymbol{V} S_i \frac{\partial}{\partial V_\ell}\mathscr{A}_i = 0, \quad \int d\boldsymbol{V} S_i \frac{\partial}{\partial V_\ell} V_\ell \mathscr{A}_i = 3dT\,\kappa_k, \tag{B 13}$$

$$\int d\boldsymbol{V} S_i \frac{\partial^2}{\partial V^2}\mathscr{A}_i = 0. \tag{B 14}$$

The right-hand side of (B 11) has already been evaluated for dry granular fluids (Garzó & Dufty 1999; Lutsko 2005) so the final form of κ_k can easily be obtained from (B 11). It is given by (7.17). The evaluation of μ_k follows mathematical steps similar to those made in the calculation of κ_k. Its explicit form can be written as

$$\mu_k = \frac{\kappa_0 \nu_0 T}{n}\left[\nu_\mu - \frac{3}{2}\left(\zeta^{(0)} - \frac{m\xi}{T}\right)\right]^{-1}\left\{\kappa_k^* \nu_0^{-1}\left[\frac{2n}{m}\gamma_n - \frac{\rho}{T}\xi_n + \zeta^{(0)}\left(1+\phi\partial_\phi \ln\chi\right)\right]\right.$$
$$+\frac{d-1}{d}a_2 + 3\frac{2^{d-2}(d-1)}{d(d+2)}\phi\chi(1+\alpha)\left(1+\frac{1}{2}\phi\partial_\phi\ln\chi\right)$$
$$\left.\times\left[\alpha(\alpha-1)+\frac{a_2}{6}(10+2d-3\alpha+3\alpha^2)\right]\right\}, \tag{B 15}$$

where

$$\nu_\mu = \frac{\int d\boldsymbol{v}\, \boldsymbol{S}(\boldsymbol{V})\cdot \mathscr{L}\boldsymbol{\mathcal{B}}(\boldsymbol{V})}{\int d\boldsymbol{v}\, \boldsymbol{S}(\boldsymbol{V})\boldsymbol{\mathcal{B}}(\boldsymbol{V})}. \tag{B 16}$$

As in the case of the shear viscosity, to get the explicit forms of ν_κ and ν_μ, one has to consider the leading terms in the (modified) Sonine polynomial expansion (Garzó *et al.* 2007*c*, 2009). To leading order the results yield $\nu_\kappa = \nu_\mu$, where μ_κ is given by (7.22).

We consider finally the first-order contribution ζ_U to the collisional cooling rate. It is given by (7.25), where ζ_{11} is defined by

$$\zeta_{11} = \frac{1}{2nT}\frac{\pi^{(d-1)/2}}{d\Gamma\left(\frac{d+3}{2}\right)}\sigma^{d-1}\chi m(1-\alpha^2)\int d\boldsymbol{V}_1 \int d\boldsymbol{V}_2\, g_{12}^3 f^{(0)}(\boldsymbol{V}_1)\mathscr{D}(\boldsymbol{V}_2), \tag{B 17}$$

where the unknown functions $\mathscr{D}(\boldsymbol{V})$ are the solutions to the linear integral equation (A 21). An approximate solution to this integral equation (A 21) can be obtained by taking the leading Sonine approximation

$$\mathscr{D}(\boldsymbol{V}) \to e_D f_M(\boldsymbol{V})F(\boldsymbol{V}), \tag{B 18}$$

where

$$F(\boldsymbol{V}) = \left(\frac{m}{2T}\right)^2 V^4 - \frac{d+2}{2}\frac{m}{T}V^2 + \frac{d(d+2)}{4}. \tag{B 19}$$

The coefficient e_D is given by

$$e_D = \frac{2}{d(d+2)}\frac{1}{n}\int \mathrm{d}\boldsymbol{V}\, \mathscr{D}(\boldsymbol{V})F(\boldsymbol{V}). \tag{B 20}$$

Substitution of (B 19) into (B 17) gives

$$\zeta_{11} = \frac{3(d+2)}{32d}\chi(1-\alpha^2)\left(1+\frac{3}{128}a_2\right)\nu_0 e_D. \tag{B 21}$$

The coefficient e_D is determined by substituting (B 22) into the integral equation (A 21), multiplying by $F(\boldsymbol{V})$ and integrating over $\boldsymbol{V}$. The result is

$$-\frac{3}{2}\left(\frac{2\gamma}{m}-\frac{m\xi}{T}+\zeta^{(0)}\right)e_D + 4\frac{\gamma}{m}e_D + \nu_\gamma e_D = \frac{2}{d(d+2)}\frac{1}{n}\int \mathrm{d}\boldsymbol{V}F(\boldsymbol{V})D(\boldsymbol{V}), \tag{B 22}$$

where the term $\zeta_{11}a_2$ has been been neglected in accordance with the present approximation. Moreover, the terms proportional to a_2 coming from ν_γ and $\zeta^{(0)}$ must also be neglected by consistency. In (B 22), we have introduced the collision frequency

$$\nu_\gamma = \frac{\displaystyle\int \mathrm{d}\boldsymbol{V}F(\boldsymbol{V})\mathscr{L}[f_M(V)F(\boldsymbol{V})]}{\displaystyle\int \mathrm{d}\boldsymbol{V}f_M(V)F(\boldsymbol{V})F(\boldsymbol{V})}. \tag{B 23}$$

As before, the right-hand side of (B 22) has been previously evaluated for dense dry granular fluids (Garzó & Dufty 1999; Lutsko 2005). Taking these results into account, the expression for e_D can be written as

$$e_D = \left(\nu_\gamma + \frac{\gamma}{m} + \frac{3m\xi}{2T} - \frac{3}{2}\zeta^{(0)}\right)^{-1}\frac{9(d+2)2^{d-8}}{d^2}\phi\chi \times\left[\frac{\omega\nu_0^{-1}}{2(d+2)} - (1+\alpha)\left(\frac{1}{3}-\alpha\right)\frac{a_2}{2}\right], \tag{B 24}$$

where ω^* and ν_γ are given by (7.28) and (7.29), respectively. With this result one gets the expression (7.27) for ζ_{11}.

Appendix C. Another theory for suspensions

In this appendix we display the explicit expressions for η and κ used by Agrawal *et al.* (2001). They can be written as $\eta = \eta_0\eta^*$ and $\kappa = \kappa_0\kappa^*$, where the (reduced) coefficients η^* and κ^* are given by

$$\eta^* = 1.2\left\{\frac{\mu_0}{\chi\delta(2-\delta)}\left(1+\frac{8}{5}\phi\delta\chi\right)\left[1+\frac{8}{5}\delta(3\delta-2)\phi\chi\right]+\frac{768}{25\pi}\delta\phi^2\chi\right\}, \tag{C 1}$$

$$\kappa^* = \frac{\lambda_0}{\chi}\left\{\left(1+\frac{12}{5}\phi\delta\chi\right)\left[1+\frac{12}{5}\delta^2(4\delta-3)\phi\chi\right]+\frac{64}{25\pi}(41-33\delta)\delta^2\phi^2\chi^2\right\}. \tag{C 2}$$

Here, we have introduced the quantities

$$\mu_0 = (1+2\beta^*)^{-1}, \quad \beta^* = \frac{5\sqrt{\pi}}{128}\frac{C_D F(\phi)}{\phi\chi}\frac{\rho_g}{\rho_s}\frac{Re_m}{Re_T}, \tag{C 3}$$

$$\lambda_0 = \frac{8}{\delta(41-33\delta)+36\beta^*}, \tag{C 4}$$

$$\delta = \frac{1+\alpha}{2}, \quad F(\phi) = (1-\phi)^{2.65}, \tag{C 5}$$

$$C_D = (24/Re_m)(1 + 0.15Re_m^{0.687}), \quad Re_m < 1000, \quad C_D = 0.44, \quad Re_m \geqslant 1000. \tag{C 6}$$

REFERENCES

ABBAS, M., CLIMENT, E. & SIMONIN, O. 2009 Shear-induced self-diffusion of inertial particles in a viscous fluid. *Phys. Rev.* E **79** (3), 036313.

AGRAWAL, K., LOEZOS, P. N., SYAMLAL, M. & SUNDARESAN, S. 2001 The role of meso-scale structures in rapid gas–solid flows. *J. Fluid Mech.* **445**, 151–185.

ANDERSON, T. B. & JACKSON, R. 1967 A fluid mechanical description of fluidized beds. *Ind. Engng Chem. Fundam.* **6**, 527–539.

BALZER, G., BOELLE, A. & SIMONIN, O. 1995 Eulerian gas–solid flow modelling of dense fluidized beds. In *Computational Gas–Solid Flows and Reacting Systems: Theory, Methods and Practice. Fluidization VIII* (ed. J. F. Large & C. Lagurie). Engineering Foundation.

BREY, J. J., DUFTY, J. W. & SANTOS, A. 1997 Dissipative dynamics for hard spheres. *J. Stat. Phys.* **87**, 1051–1066.

BREY, J. J., DUFTY, J. W., SANTOS, A. & KIM, C. S. 1998 Hydrodynamics for granular flows at low density. *Phys. Rev.* E **58**, 4638–4653.

BRILLIANTOV, N. & PÖSCHEL, T. 2004 *Kinetic Theory of Granular Gases*. Oxford University Press.

CAMPBELL, C. S. 1990 Rapid granular flows. *Annu. Rev. Fluid Mech.* **22**, 57–92.

CARNAHAN, N. F. & STARLING, K. E. 1969 Equation of state for nonattracting rigid spheres. *J. Chem. Phys.* **51**, 635–636.

CHAPMAN, S. & COWLING, T. G. 1970 *The Mathematical Theory of Nonuniform Gases*. Cambridge University Press.

CLEMENT, C. P., PACHECO-MARTÍNEZ, H. A., SWIFT, M. R. & KING, P. J. 2010 The water-enhanced Brazil nut effect. *Europhys. Lett.* **91**, 54001.

FÉVRIER, P., SIMONIN, O. & SQUIRES, K. D. 2005 Partitioning of particle velocities in gas–solid turbulent flows into a continuous field and a spatially uncorrelated random distribution: theoretical formalism and numerical study. *J. Fluid. Mech.* **533**, 1–46.

GARDINER, C. W. 1985 *Handbook of Stochastic Methods*, second edition. Springer.

GARZÓ, V. 2005 Instabilities in a free granular fluid described by the Enskog equation. *Phys. Rev.* E **72**, 021106.

GARZÓ, V. & DUFTY, J. W. 1999 Dense fluid transport for inelastic hard spheres. *Phys. Rev.* E **59**, 5895–5911.

GARZÓ, V., DUFTY, J. W. & HRENYA, C. M. 2007*a* Enskog theory for polydisperse granular mixtures. Part 1. Navier–Stokes order transport. *Phys. Rev.* E **76**, 031303.

GARZÓ, V., HRENYA, C. M. & DUFTY, J. W. 2007*b* Enskog theory for polydisperse granular mixtures. Part 2. Sonine polynomial approximation. *Phys. Rev.* E **76**, 031304.

GARZÓ, V. & SANTOS, A. 2003 *Kinetic Theory of Gases in Shear Flows: Nonlinear Transport*. Kluwer Academic.

GARZÓ, V., SANTOS, A. & MONTANERO, J. M. 2007*c* Modified Sonine approximation for the Navier–Stokes transport coefficients of a granular gas. *Physica* A **376**, 94–107.

GARZÓ, V., VEGA REYES, F. & MONTANERO, J. M. 2009 Modified Sonine approximation for granular binary mixtures. *J. Fluid Mech.* **623**, 387–411.

GIDASPOW, D. 1994 *Multiphase Flow and Fluidization*. Academic.

GIDASPOW, D. & JIRADILOK, V. 2009 *Computational Techniques: The Multiphase CFD Approach to Fluidization and Green Energy Technologies*. Nova.

GOLDHIRSCH, I. 2003 Rapid granular flows. *Annu. Rev. Fluid Mech.* **35**, 267–293.

HRENYA, C. M., GALVIN, J. E. & WILDMAN, R. D. 2008 Evidence of higher-order effects in thermally driven granular flows. *J. Fluid Mech.* **598**, 429–450.

IDLER, V., SÁNCHEZ, I., PAREDES, R., GUTIÉRREZ, G., REYES, L. I. & BOTET, R. 2009 Three-dimensional simulations of a vertically vibrated granular bed including interstitial air. *Phys. Rev.* E **79**, 051301.

JACKSON, R. 2000 *The Dynamics of Fluidized Particles*. Cambridge University Press.

KOCH, D. L. 1990 Kinetic theory for a monodisperse gas–solid suspension. *Phys. Fluids* A **2**, 1711–1723.

KOCH, D. L. & HILL, R. J. 2001 Inertial effects in suspensions and porous-media flows. *Annu. Rev. Fluid Mech.* **33**, 619–647.

KOCH, D. L. & SANGANI, A. S. 1999 Particle pressure and marginal stability limits for a homogeneous monodisperse gas-fluidized bed: kinetic theory and numerical simulations. *J. Fluid Mech.* **400**, 229–263.

LUMLEY, J. L. & NEWMAN, G. R. 1977 The return to isotropy of homogeneous turbulence. *J. Fluid Mech.* **82**, 161–178.

LUN, C. K. K. & SAVAGE, S. B. 2003 Kinetic theory for inertia flows of dilute turbulent gas–solids mixtures. In *Granular Gas Dynamics* (ed. T. Pöschel & N. Brilliantov), p. 263. Springer.

LUTSKO, J. 2005 Transport properties of dense dissipative hard-sphere fluids for arbitrary energy loss models. *Phys. Rev.* E **72**, 021306.

MA, D. & AHMADI, G. 1988 A kinetic model for rapid granular flow of nearly elastic particles including interstitial fluid effects. *Powder Technol.* **56**, 191–207.

MÖBIUS, M. E., CHENG, X., ESHUIS, P., KARCZMAR, G. S., NAGEL, S. R. & JAEGER, H. M. 2005 Effect of air on granular size separation in a vibrated granular bed. *Phys. Rev.* E **72**, 011304.

MÖBIUS, M. E., LAUDERDALE, B. E., NAGEL, S. R. & JAEGER, H. M. 2001 Size separation of granular particles. *Nature (London)* **414**, 270.

MONTANERO, J. M. & SANTOS, A. 2000 Computer simulation of uniformly heated granular fluids. *Granul. Matt.* **2**, 53–64.

MONTANERO, J. M., SANTOS, A. & GARZÓ, V. 2007 First-order Chapman–Enskog velocity distribution function in a granular gas. *Physica* A **376**, 75–93.

NAYLOR, M. A., SWIFT, M. R. & KING, P. J. 2003 Air-driven Brazil nut effect. *Phys. Rev.* E **68**, 012301.

VAN NOIJE, T. P. C. & ERNST, M. H. 1998 Velocity distributions in homogeneous granular fluids: the free and heated case. *Granul. Matt.* **1**, 57–64.

PANNALA, S., SYAMLAL, M. & O'BRIEN, T. J. 2011 *Computational Gas–Solids Flows and Reacting Systems: Theory, Methods and Practice*. doi:10.4018/978-1-61520-651-3.

PÖSCHEL, T. & BRILLIANTOV, N. 2006 Breakdown of the Sonine expansion for the velocity distribution of granular gases. *Europhys. Lett.* **74**, 424–430.

RERICHA, E. C., BIZON, C., SHATTUCK, M. D. & SWINNEY, H. L. 2002 Shocks in supersonic sand. *Phys. Rev. Lett.* **88**, 014302.

RICHARDSON, J. F. & ZAKI, W. N. 1954 Sedimentation and fluidisation. Part 1. *Trans. Inst. Chem. Engrs Lond.* **32**, 35.

SÁNCHEZ, P., SWIFT, M. R. & KING, P. J. 2004 Stripe formation in granular mixtures due to the differential influence of drag. *Phys. Rev. Lett.* **93**, 184302.

SANGANI, A. S., MO, G., TSAO, H.-K. & KOCH, D. L. 1996 Simple shear flows of dense gas–solid suspensions at finite Stokes numbers. *J. Fluid Mech.* **313**, 309–341.

SANTOS, V., GARZÓ, V. & DUFTY, J. W. 2004 Inherent rheology of a granular fluid in uniform shear flow. *Phys. Rev.* E **69**, 061303.

SANTOS, A. & MONTANERO, J. M. 2009 The second and third Sonine coefficients of a freely cooling granular gas revisited. *Granul. Matt.* **11**, 157–168.

SIMONIN, O., ZAICHIK, L. I., ALIPCHENKOV, V. M. & FÉVRIER, P. 2006 Connection between two statistical approaches for the modelling of particle velocity and concentration distributions in turbulent flow: the mesoscopic Eulerian formalism and the two-point probability density function method. *Phys. Fluids* **18** (12), 125107.

SINCLAIR, J. L. & JACKSON, R. 1989 Gas-particle flow in a vertical pipe with particle–particle interactions. *AIChE J.* **35**, 1473–1486.

SUNDARAM, S. & COLLINS, L. R. 1999 A numerical study of the modulation of isotropic turbulence by suspended particles. *J. Fluid Mech.* **379**, 105–143.

TENNETI, S., FOX, R. O. & SUBRAMANIAM, S. 2010*a* Instantaneous particle acceleration model for gas–solid suspensions at moderate Reynolds numbers. In *7th International Conference on Multiphase Flow*, Tampa, Florida. http://ufdc.ufl.edu/UF00102023/00189.

TENNETI, S., GARG, R., HRENYA, C. M., FOX, R. O. & SUBRAMANIAM, S. 2010*b* Direct numerical simulation of gas–solid suspensions at moderate Reynolds number: quantifying the coupling between hydrodynamic forces and particle velocity fluctuations. *Powder Technol.* **203**, 57–69.

TSAO, H.-K. & KOCH, D. L. 1995 Simple shear flows of dilute gas–solid suspensions. *J. Fluid Mech.* **296**, 211–245.

WEN, C. Y. & YU, Y. H. 1966 Mechanics of fluidization. *Chem. Engng Prog. Symp. Ser.* **62**, 100–111.

WILDMAN, R., MARTIN, T. W., HUNTLEY, J. M., JENKINS, J. T., VISWANATHAN, H., FEN, X. & PARKER, D. J. 2008 Experimental investigation and kinetic-theory-based model of a rapid granular shear flow. *J. Fluid Mech.* **602**, 63–79.

WYLIE, J. J., ZHANG, Q., XU, H. Y. & SUN, X. X. 2008 Drag-induced particle segregation with vibrating boundaries. *Europhys. Lett.* **81**, 54001.

XU, Y. & SUBRAMANIAM, S. 2006 A multiscale model for dilute turbulent gas-particle flows based on the equilibration of energy concept. *Phys. Fluids* **18**, 033301.

YAN, X., SHI, Q., HOU, M., LU, K. & CHAN, C. K. 2003 Effects of air on the segregation of particles in a shaken granular bed. *Phys. Rev. Lett.* **91**, 014302.

ZAICHIK, L. I., SIMONIN, O. & ALIPCHENKOV, V. M. 2009 An Eulerian approach for large eddy simulation of particle transport in turbulent flows. *J. Turbul.* **10** (4), 1–21.

ZEILSTRA, M. A., VAN DER HOEF, M. A. & KUIPERS, J. A. M. 2008 Simulations of density segregation in vibrated beds. *Phys. Rev.* E **77**, 031309.